



**HAL**  
open science

# Production of Purified H<sub>2</sub>, Heat, and Biochar from Wood: Comparison between Gasification and Autothermal Pyrolysis Based on Advanced Process Modeling

Rémi Demol, Anthony Dufour, Yann Rogaume, Guillain Mauviel

► **To cite this version:**

Rémi Demol, Anthony Dufour, Yann Rogaume, Guillain Mauviel. Production of Purified H<sub>2</sub>, Heat, and Biochar from Wood: Comparison between Gasification and Autothermal Pyrolysis Based on Advanced Process Modeling. *Energy & Fuels*, 2021, 36 (1), pp.488-501. 10.1021/acs.energyfuels.1c03528 . hal-03540835

**HAL Id: hal-03540835**

**<https://hal.science/hal-03540835>**

Submitted on 18 Apr 2023

**HAL** is a multi-disciplinary open access archive for the deposit and dissemination of scientific research documents, whether they are published or not. The documents may come from teaching and research institutions in France or abroad, or from public or private research centers.

L'archive ouverte pluridisciplinaire **HAL**, est destinée au dépôt et à la diffusion de documents scientifiques de niveau recherche, publiés ou non, émanant des établissements d'enseignement et de recherche français ou étrangers, des laboratoires publics ou privés.

1                   **Production of purified H<sub>2</sub>, heat and bio-char from wood:**  
2                   **comparison between gasification and auto-thermal pyrolysis**  
3                   **based on advanced process modeling**

4                   Rémi DEMOL<sup>1</sup>, Anthony DUFOUR<sup>1</sup>, Yann ROGAUME<sup>2</sup>, Guillain MAUVIEL<sup>1,\*</sup>.

5                   1. Université de Lorraine, CNRS, Fédération J. Villermaux, 1 rue Grandville, 54000 Nancy, France.

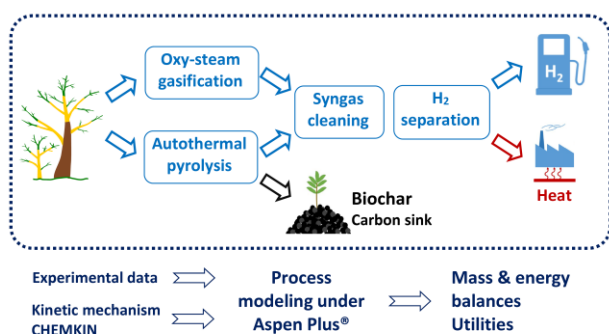
6                   2. Université de Lorraine, CNRS, Fédération J. Villermaux, 27 rue Philippe Séguin, 88000 Epinal,  
7                   France.

8                   \*Corresponding author: guillain.mauviel@univ-lorraine.fr (G. Mauviel)

9                   <https://doi.org/10.1021/acs.energyfuels.1c03528>

11                   **TOC GRAPHIC**

12                   8.16cm\*4.45cm



15                   **ABSTRACT**

16                   Biomass gasification is an interesting route for renewable hydrogen production, but it is still hampered  
17                   by technical, environmental and economic issues. A first key step toward its development is the  
18                   quantification of mass and energy balances of the integrated process. This work compares different  
19                   processes to produce a purified H<sub>2</sub> from wood but also other products (heat, bio-char) at medium scale  
20                   power (20 MW of biomass power inlet that corresponds to 3.7 t<sub>dry</sub>/h). Three complementary processes  
21                   were modeled under Aspen Plus including biomass drying, gasification-pyrolysis reactors and advanced  
22                   syngas upgrading units. The first two cases are based on oxygen/steam gasification 1) with or 2)  
23                   without catalytic reactors (steam reforming and water gas-shift). The third case is an autothermal

24 oxidative pyrolysis resulting in bio-char and syngas. All the syngas cleaning process was detailed with  
25 a special focus on a partial oxidation (POX) unit to reduce the tar content. This unit was modeled by  
26 coupling Aspen Plus with Chemkin to predict tar and syngas composition by detailed elementary  
27 mechanisms. A hybrid hydrogen separation process is proposed combining membrane and pressure  
28 swing adsorption. A cape-open module for membrane modeling (called Memsic) was included in the  
29 whole process model. The global energetic efficiency is 75.4, 77.8 and 80.4%net for scenarios 1, 2 and  
30 3, respectively. The hydrogen yields are 79, 26 and 18  $\text{g}_{\text{H}_2}/\text{kg}_{\text{biomass,dry}}$  after separation and heat  
31 efficiencies - corresponding to hot water production - were 23.4, 60.0 and 49.0%net respectively. The  
32 option 3 produces 110  $\text{g}_{\text{biochar}}/\text{kg}_{\text{biomass,dry}}$  which is a carbon sink. All utilities and consumables were  
33 also determined. This model can be used for techno-economic and life cycle assessment studies. This  
34 methodology is also of interest to model all other thermochemical processes with detailed kinetics  
35 embedded in process models.

## 36 1. INTRODUCTION

37 Biomass is used for centuries to fulfill the heat and material demand for human activities. It is  
38 historically and even nowadays the first renewable energy<sup>1,2</sup>. The growing concerns about climate  
39 change resulting from anthropogenic emissions and the fore casted peak in oil production pushes  
40 researchers to develop innovative processes for the production of energy commodities from  
41 renewables. The taxation of greenhouse gas emissions is expected to favor the development of carbon-  
42 neutral or even carbon-negative processes<sup>3,4</sup>.

43 Among the ways to decarbonize human activities, hydrogen knows a growing interest for mobility  
44 applications and for lowering industry carbon intensity<sup>5</sup>. Yet, even if this fuel does not release carbon  
45 dioxide during its combustion, its production—mainly from steam methane reforming, does. If H<sub>2</sub> is  
46 produced from water electrolysis, the CO<sub>2</sub> emission problem is then related to the electricity  
47 generation processes. Different policies tend to promote renewable hydrogen. France fixed the  
48 objective to increase the share of renewable hydrogen to 20–40% in 2028 in the industry sector<sup>6</sup>.  
49 Besides water electrolysis from renewable electricity, the thermochemical processes also provide a  
50 potential way to produce hydrogen from biomass.

51 The gasification is the partial oxidation of a solid feedstock to produce a synthetic gas (syngas) made  
52 of CO, H<sub>2</sub>, CO<sub>2</sub>, CH<sub>4</sub>, H<sub>2</sub>O and light hydrocarbons. Polycyclic aromatic hydrocarbons (PAHs), NH<sub>3</sub>, HCl,  
53 H<sub>2</sub>S are also formed and must be removed from the syngas before its upgrading<sup>7</sup>. The gasifying agent  
54 could be steam in order to maximize the concentration of hydrogen but it leads to highly endothermic  
55 behavior. The use of air leads to syngas diluted with nitrogen when the gasification is direct: this option  
56 should be avoided because it hampers the H<sub>2</sub> purification. To overcome this problem, a dual fluidized  
57 bed can be used<sup>8,9</sup> but it results in a complex technology notably due to loop seals<sup>10</sup>. Another way is to  
58 use pure oxygen and steam instead of air<sup>11</sup>. In any cases, the fluidized bed temperature is typically  
59 higher than 750°C to convert the pyrolysis char into syngas<sup>12</sup>.

60 Another thermochemical process can produce hydrogen: the pyrolysis, that may also be achieved in  
61 fluidized bed<sup>13,14</sup>. This process produces char, tar and permanent gas. To overcome the endothermicity  
62 of pyrolysis, a small amount of oxygen can be added to reach autothermal conditions<sup>15</sup>. But this  
63 pyrolysis step alone does not lead to high H<sub>2</sub> yields. In this article, it is proposed to do the partial  
64 oxidation of the tar and gas produced by pyrolysis in a downstream gas-phase reactor. This second  
65 step is achieved by mixing oxygen with pyrolysis gas in a partial oxidation (POX) reactor to reach high  
66 temperature (> 1000°C), thus producing a H<sub>2</sub>-rich syngas. Furthermore, the bio-char produced in the  
67 pyrolysis reactor enables carbon sequestration<sup>3,16</sup>.

68 The hydrogen in the syngas is relatively diluted (even with oxy-steam gasification) in the range 30–  
69 45%vol on a dry basis<sup>11,17,18</sup>. The production of hydrogen at high purity is difficult at this concentration  
70 for standard separation unit. Pressure swing adsorption (PSA H<sub>2</sub>) is the classical technology. More than  
71 70%vol of H<sub>2</sub> are required at the inlet<sup>19</sup>. To increase the content of H<sub>2</sub>, a reformer and water-gas-shift  
72 catalytic reactors should be added<sup>11,20–22</sup>. These reactors can be positioned after cold syngas  
73 cleaning<sup>4,20,23</sup>, or rather, downstream the gasifier to promote heat integration. The use of catalytic  
74 reactors after a gasifier has been demonstrated with catalytic reformers<sup>24,25,11</sup> and CO-shift catalytic  
75 reactors<sup>11,21,22,26</sup>. The tar content must be reduced below 2 g/Nm<sup>3</sup> dry basis (including benzene) at high  
76 temperature to avoid catalyst deactivation<sup>25</sup>. No deactivation from H<sub>2</sub>S was observed below  
77 100 ppm<sup>11</sup>.

78 The harvesting area of the biomass should be limited to minimize the economic and environmental  
79 impacts of its transport. Besides another argument for relatively small-scale biomass conversion  
80 process is linked to the fact that heat produced by the process should be valorized locally in order to  
81 increase the global efficiency<sup>27</sup>. It is clearly easier to find a location for biomass gasifiers with a small  
82 heat demand (few MW) than a large one (dozens of MW). Finally, a local production of H<sub>2</sub> might be  
83 preferred for more direct and decentralized H<sub>2</sub> station for transport or industrial sectors, instead of a  
84 centralized production with H<sub>2</sub> transport by trucks<sup>28</sup>.

85 The whole pyrogasification process must be modeled, from biomass drying to hydrogen separation, in  
86 order to assess the potential of the production of hydrogen from biomass. The study must also include  
87 co-products recovery and waste treatment. The modeling of pyrogasification processes has already  
88 been conducted, especially for the cleaning and conditioning of the syngas<sup>27,29</sup> and also for hydrogen  
89 production at large-scale facilities<sup>19,20</sup>. Gasification is often modeled as a combination of RYIELD and  
90 RGIBBS reactors. Firstly, the biomass is decomposed into its elemental stable components (H<sub>2</sub>, C, O<sub>2</sub>,  
91 N<sub>2</sub>, H<sub>2</sub>S, HCl). Then the RGIBBS reactor estimates the equilibrium composition at a given temperature<sup>30</sup>.  
92 This model can give a rough estimate of the main components but it is unable to predict the yields of  
93 minor products (tars) which are the bottleneck of gasification. The tar formation and up-grading has  
94 been modeled but the chosen models are frequently overly simplistic<sup>31</sup>. Some research groups  
95 developed a fluidized bed model to predict the main products and some secondary products<sup>32–34</sup>.

96 To the best of our knowledge, advanced models of the complete process, from biomass to purified H<sub>2</sub>,  
97 are still scarce, notably if one considers tar formation and upgrading.

98 Spath et al. has studied in a pioneering work the modeling of the complete process of hydrogen  
99 production from biomass gasification in an indirectly-heated gasifier. The steam reformer and water  
100 gas-shift reactors was positioned after wet scrubbing of tars inducing a heat penalty on the process<sup>20</sup>.

101 The scale (2000 dry ton/day) of this process makes possible the use of catalytic reactors but it requires  
102 long-distance collection of biomass. They used empirical correlations to model syngas and tar  
103 composition.

104 Martín and Grossmann presented the basis of a superstructure optimization for the production of  
105 Fischer-Tropsch diesel from biomass<sup>35</sup>. The optimal solution to reach the targeted CO/H<sub>2</sub> ratio was  
106 composed of an indirect gasifier and a steam reformer instead of direct gasification coupled to partial  
107 oxidation. No further composition adjustment (water gas-shift, PSA H<sub>2</sub>) was necessary for this  
108 application<sup>35</sup>.

109 Syngas cleaning and upgrading processes usually consist in tar reformer, water gas-shift reactor and  
110 PSA H<sub>2</sub><sup>36-40</sup>, possibly with Sulphur removal with a chelated iron solution (LO-CAT process)<sup>41</sup>. The tar  
111 reformer can be replaced by catalytic filter candles<sup>42</sup>. When tars species were considered, only few  
112 surrogate molecules were included<sup>36,42</sup>. The purified H<sub>2</sub> yield was estimated to 76.1<sup>36</sup>, 55.0<sup>41</sup>, 75.2<sup>42</sup> or  
113 107.4<sup>37</sup> g<sub>H<sub>2</sub></sub>/kg<sub>biomass</sub>. On an energetic basis, Kalinci et al. showed that gasifier and PSA exhibit the most  
114 energy and exergy losses along the process<sup>38</sup>.

115 Marcantonio et al. modeled a circulating bubbling fluidized bed with a quasi-equilibrium approach  
116 model validated on experimental data from a pilot plant. They also investigated the use of a palladium  
117 membrane that gave a better H<sub>2</sub> recovery<sup>43</sup>.

118 The purification of the syngas was investigated in more details with Ribeiro et al. by modeling the  
119 detailed PSA cycle to remove CO<sub>2</sub> from the syngas. H<sub>2</sub> and CO were dedicated for Fischer-Tropsch fuels  
120 production<sup>44</sup>. To the best of our knowledge, no model was published on membrane combined with  
121 PSA for H<sub>2</sub> separation.

122 Our research group has developed previous Aspen Plus® models about biomass gasification and  
123 oxidation<sup>27,29,32,45,46</sup> for heat or power production. Here, we complete our previous work on different  
124 pyro-gasification processes dedicated to the production of purified hydrogen and bio-char, with  
125 different gasification reactors and syngas refining units. We have also improved our modeling  
126 approach by including detailed kinetic mechanisms embedded under Aspen Plus.

127 The aim of this work is to provide detailed mass and energy balances for three processes along with  
128 utilities and consumables. These data are essential for further techno-economic and environmental  
129 assessment.

130 The first scenario considers the maximization of hydrogen production and a residual heat production.  
131 The second one is a simpler and probably cheaper process with lower hydrogen production but higher

132 heat production. The third case is based on oxidative pyrolysis to produce bio-char (carbon sink),  
133 hydrogen and heat. All these options were modeled in Aspen Plus® associated with experimental data  
134 obtained from the literature and from a semi-industrial pilot plant (University of Lorraine, Epinal,  
135 France)<sup>47</sup>.

136 Therefore, the novelty of this work can be outlined by these three main aspects:

- 137 1) To the best of our knowledge, these three processes were not yet modeled with the proposed  
138 detailed approach under the Aspen Plus framework, including elementary reactions for gas-  
139 phase reactions, hydrodynamic of fluidized bed, and advanced purification of H<sub>2</sub> (membrane  
140 permeation and PSA adsorption).
- 141 2) Novel results on gas cleaning in a Venturi scrubber on a gasification pilot plant are presented  
142 and embedded in the Aspen Plus model.
- 143 3) These three main routes of H<sub>2</sub>, heat and bio-char production are compared and discussed  
144 based on their energy, mass and hydrogen balance.

145

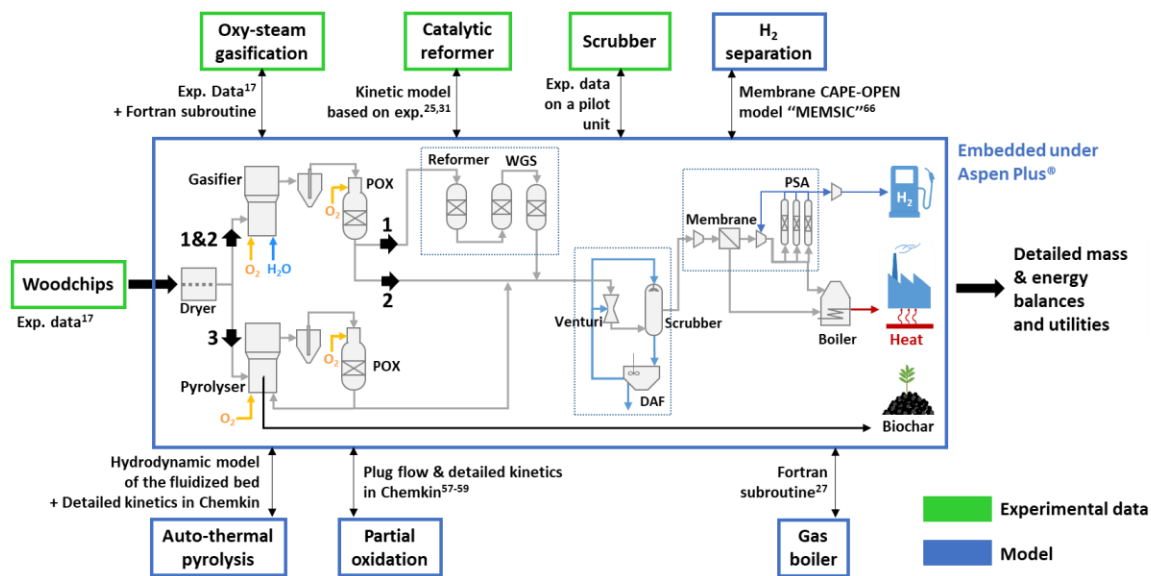
146 **2. MODEL DESCRIPTION**

147 **2.1. Scenarios investigated**

148 Three scenarios of hydrogen production from biomass were investigated (Figure 1). The three  
 149 scenarios were designed for a territorial scale of 20 MW LHV-basis (30 kt dry biomass/year). The  
 150 gasifier is a single fluidized bed reactor, which is cheaper and simpler to manage at territorial scale in  
 151 comparison to dual fluidized bed technology. The gasifying agent is a mixture of oxygen and steam.  
 152 Case 1 aims at maximizing the production of H<sub>2</sub> by implementing a steam reformer and water-gas shift  
 153 catalytic reactors downstream the fluidized bed. It is based on experimental results of Corella et al.<sup>11</sup>.  
 154 Case 2 considers a simpler process without catalytic reactors, targeting a lower production of H<sub>2</sub> and a  
 155 higher production of heat. The last case investigates the autothermal pyrolysis of biomass to produce  
 156 bio-char and a H<sub>2</sub>-rich gas obtained after the partial oxidation of the pyrolysis gas.

157 **2.2. Description of the processes and modeling**

158 The modeling approach is presented in Figure 1.



159  
 160 **Figure 1: Simplified process flow diagram and the various modeling approach for each units.**

161  
 162 Our model under Aspen Plus 8.8® handles a combination of experimental data, which were preferred  
 163 when available, and of more fundamental modeling based on kinetics (for gas-phase or catalytic  
 164 reactions) or on mass transfers (membrane) when experimental results on biomass real syngas were  
 165 not available.

166 Figure 1 presents a simplified flow sheet of the 3 cases and Figure 2 the detailed flow sheet for case 1.  
167 The main assumptions of each process units are summarized in Table 2 and discussed here after.

168 The feedstock considered was woodchips, a by-product of the forest harvesting and wood industry.  
169 This biomass was supposed to be crushed directly in the forest or in dedicated platforms. The humidity  
170 was fixed to 40%wt after delivery. Table S1 provides the detailed composition of the feedstock.

171 The detailed flow sheets of the three options are presented in supporting information (SI) (Figure S1-  
172 S3). The equation of state RK-Aspen was used as it is recommended for hydrocarbon mixtures and light  
173 gases<sup>48</sup>. The species BIOMASS and CHAR were modeled as non-conventional solids with their  
174 proximate and elemental composition. The heat of combustion was estimated with Mott and Spooner  
175 model, which is tailored for biomass and its high oxygen content<sup>49</sup>.

### 176 **2.2.1. Biomass drying**

177 The biomass was considered dried down to 20%wt with the low-temperature heat contained in the  
178 boiler exhaust gas in order to increase energy efficiency and to limit the amount of tars produced by  
179 the gasifier<sup>50</sup>. The dryer model was taken from François et al.<sup>27</sup>. It estimates the VOCs emissions during  
180 the drying.

### 181 **2.2.2. Oxygen production**

182 Concerning the production of oxygen as gasifying agent, the VSA O<sub>2</sub> (vacuum swing adsorption) process  
183 is the most adapted one for small-scale production in the range of 10 to 200 tons of O<sub>2</sub> per day and if  
184 very highly pure O<sub>2</sub> is not required (93-95%v, the rest is mainly argon)<sup>51</sup>. The VSA O<sub>2</sub> was modeled as a  
185 simple separator to reach a purity of 93%v and a recovery rate of 55%<sup>52</sup>. Air was compressed at 1.5 bar  
186 before the columns. The purge pressure was set to 0.6 bar obtained with a vacuum pump. An  
187 adsorbent commonly used consists of lithium-doped zeolites. The required adsorbent quantity was  
188 estimated from ref.<sup>53</sup>.

### 189 **2.2.3. Gasifier**

190 The gasification and the pyrolysis were conducted in a bubbling fluidized bed, which is the most  
191 adapted technology for the targeted scale<sup>54</sup>.

192 For cases 1 and 2, a real syngas composition from literature data was used in order to have a detailed  
193 and accurate composition of tars. Among few detailed results available in literature<sup>17,18</sup>, the  
194 experimental results obtained by Schmid et al.<sup>17</sup> in a steam/oxygen fluidized bed were selected (see SI  
195 S2). Their operating conditions were tailored to the production of hydrogen with an equivalent ratio  
196 (ER) of 0.25 and a molar steam to carbon ratio of 1 for a bed temperature at 850°C. The solid organic

197 residue (char) yield was estimated to 10 g daf/kg of dry biomass. Gil et al. mentioned 5-20g/kg daf as  
198 char yield for a steam-oxygen bubbling fluidized bed<sup>55</sup>. Therefore, 10 g daf/kg dry biomass of char is  
199 an average common value for char yield produced by this technology. The elemental composition of  
200 char was assumed as: 85% C, 2% H and 13% O daf. The global solid residue recovered is made up of  
201 char and ash. An external Fortran subroutine linked to RYIELD model was used to compute the gas and  
202 tar composition according to the experimental results and to the biomass flow rate. Atomic balances  
203 in C, H, O, Cl and S were ensured by adjusting the CO<sub>2</sub>, H<sub>2</sub>O, O<sub>2</sub>, HCl and H<sub>2</sub>S flows, respectively. The  
204 heat balance was used in the RYIELD model to calculate the temperature of the syngas at the outlet  
205 assuming an adiabatic reactor.

#### 206 **2.2.4. Pyrolyser**

207 In the case 3, an adiabatic fluidized bed pyrolyser was used. A small amount of oxygen was injected  
208 (auto-thermal conditions) to provide heat internally<sup>15</sup>. As a consequence, its behavior was very close  
209 to the auto-thermal fluidized bed gasifier used in the first scenarios. The main difference was the bed  
210 temperature below 600°C instead of 850°C. In this condition, pyrolysis char was an important product  
211 to be recovered. To the best of the author's knowledge, no detailed data on the auto-thermal pyrolysis  
212 presenting gas molecular composition (gas and tar) is available in the literature. Therefore, in order to  
213 model this auto-thermal pyrolysis, a model was developed to estimate the yield and detailed  
214 composition of pyrolysis products (char, gas, water and tars). Ranzi's model of biomass pyrolysis<sup>56</sup> and  
215 radical kinetic mechanisms<sup>57-59</sup> were used. The ER used was set to 0.10, slightly higher than the  
216 minimum ER of 0.08 estimated by Brown for autothermal pyrolysis at around 500°C to compensate  
217 heat losses<sup>15</sup>. The heat balance showed that an ER equals to 0.10 was able to reach a mean  
218 temperature in the fluidized bed of 565°C. Additional information on the pyrolysis model and a  
219 comparison with experimental results can be found in SI S3. A part of the syngas was recycled to the  
220 fluidized bed to maintain a fluidization velocity consistent to the gasification cases. An external Fortran  
221 subroutine was used to ensure mass balance similarly to the gasification reactor.

#### 222 **2.2.5. Partial oxidation, steam reformer and water-gas shift**

223 When the production of H<sub>2</sub> is maximized (case 1), the process includes catalytic steam reformer and  
224 water gas shift units. These two steps were conducted at high temperature after the gasifier in order  
225 to promote heat integration and according to the experiments of Corella et al.<sup>11</sup>. Unfortunately, the  
226 catalysts are sensitive to the concentration of tars which may cause their deactivation. 2 g/Nm<sup>3</sup>  
227 (including benzene, dry basis) was recommended by Corella et al. as the targeted tar content for  
228 maintaining the stability of the catalytic reformer<sup>25</sup>. Therefore, a partial oxidizing unit was used after  
229 the gasifier to reduce the tar content down to 2g/Nm<sup>3</sup>. This limit can also be obtained by an optimized

230 design and operation of the gasifier even if it was not the case with the experimental data used here  
231 for syngas composition since olivine was used as bed material. A better catalyst (dolomite, nickel-  
232 olivine) can contribute to the reduction of tar content, but it would also increase the operating costs.  
233 The addition of a small amount of oxygen in the syngas leads to the oxidation and cracking of tars at  
234 high temperature (over 1000°C). This POX unit was modeled by detailed kinetic models<sup>57–59</sup> which were  
235 implemented by coupling Aspen Plus with ANSYS Chemkin Pro 17.0 (SI S4). For the gasification  
236 scenarios (1-2), the oxygen was adjusted to an equivalent ratio of 0.12 to reach the target of 2 g/Nm<sup>3</sup>  
237 of tars. More details on the impact of this ER are given in SI, section S5.

238 Experiments on steam reforming and water-gas-shift with a real syngas were conducted in the  
239 literature<sup>25,60</sup>. The reformer reactor was modeled with RPLUG and the kinetics of Corella's team<sup>25</sup> with  
240 a nickel-based catalyst (reactions and kinetics presented in SI S6). The dimensions of the reactor were  
241 adjusted to reach 95% conversion of methane according to Caballero et al.<sup>24</sup>. This kinetic approach  
242 allowed to predict the remaining tars after the catalytic reformer.

243 Then, two stages of water gas shift were used, first at high temperature (350°C), second at a lower  
244 temperature (200°C) to promote CO conversion. The catalysts commonly used are iron/chromium  
245 oxide and Cu/ZnO/Al<sub>2</sub>O<sub>3</sub> for high and low temperature respectively<sup>11</sup>. The water-gas-shift reactors  
246 were modeled with RGIBBS model and a temperature approach of 20°C<sup>20</sup>. A steam to CO ratio of 3 was  
247 used to maximize the H<sub>2</sub> production.

#### 248 **2.2.6. Wet scrubbing of syngas**

249 As a final syngas polishing, water scrubber was chosen to remove residual tars and other contaminants  
250 (NH<sub>3</sub>, HCl, H<sub>2</sub>S). Even if this operation was not required for tar removal in case 1, the wet scrubber has  
251 another purpose: the condensation of the syngas water content. Table 1 presents the tar removal  
252 efficiency found in literature and based on a pilot system experiment with Venturi and wet scrubbers  
253 in series. This pilot plant at University of Lorraine (Epinal, France) can operate 50 kg biomass/h. The  
254 scrubbing water flow rate is about 1 m<sup>3</sup>/h.

255 This step was modeled as a FLASH unit and the composition of tars adjusted accordingly to the  
256 experimental results (of Table 1). The removal of NH<sub>3</sub>, H<sub>2</sub>S and HCl was modeled with ELECNRTL  
257 model<sup>27</sup>.

#### 258 **2.2.7. Wastewater treatment**

259 The species removed from the syngas and present in the scrubbing water were separated by  
260 coagulation and flotation in a dissolved air flotation unit (DAF) with the addition of soda to increase

261 the pH along with flocculants and coagulant. The excess of water resulting from condensing water from  
 262 the syngas was removed and sent to district water system after a fixed bed of activated carbon to  
 263 remove the residual contaminants<sup>61,62</sup>. The amount of activated carbon was estimated with ref. <sup>62</sup>.

264 **Table 1: Wet scrubber efficiency.**

	<b>Pilot plant, this work (Venturi + wet scrubber)<sup>a</sup></b>	<b>Rabou et al. (2009)<sup>63</sup> Water absorber</b>
Benzene	0%	35%
<b>Class 2<sup>b</sup></b>	<b>44% (global<sup>c</sup>)</b>	72%
o-Xylene	9%	
Phenol	99%	
o-Cresol	33%	
m,p-Cresol	100%	
<b>Class 3<sup>b</sup></b>	<b>4% (global<sup>c</sup>)</b>	28%
Toluene	4%	
<b>Class 4<sup>b</sup></b>	<b>70% (global<sup>c</sup>)</b>	69%
Indene	37%	
Naphthalene	58%	
2-methylNaphthalene	80%	
1-methylNaphthalene	82%	
Acenaphthylene	91%	
Acenaphthene	97%	
Fluorene	100%	
Phenanthrene	95%	
Anthracene	100%	
Fluoranthene	100%	
<b>Class 5<sup>b</sup></b>	<b>100% (global<sup>c</sup>)</b>	50%
Pyrene	100%	

<sup>a</sup>Syngas temperature around 150°C and 30°C at the inlet and outlet respectively, scrubbing water between 25 and 35°C at the inlet and outlet respectively.

<sup>b</sup>ECN classification<sup>64</sup>.

<sup>c</sup>This value is an average that takes into account the relative yields of tars in this class.

265

266 **2.2.8. Hydrogen separation**

267 The standard process for H<sub>2</sub> separation is the pressure swing adsorption unit (PSA). Yet, the inlet  
 268 concentration of H<sub>2</sub> should be at least 70%v to reach a high purity separation (99.99%v)<sup>20</sup>. To achieve  
 269 such high concentration at the inlet, a part of the pure hydrogen produced can be recycled at the inlet  
 270 of the PSA<sup>20</sup>. However, when the concentration of H<sub>2</sub> was too low (cases 2 and 3), a polyimide  
 271 membrane permeable to H<sub>2</sub> was used before the PSA. The membrane plays the role of a H<sub>2</sub> pre-  
 272 concentrator (more details are given in SI S7).

273 The PSA was modeled as a SEP block with fixed recovery and purity, a part of the product was recycled  
 274 to reach 70%v content in H<sub>2</sub><sup>20</sup>. The recovery rate was assumed to be 85%. The amount of adsorbent

275 (zeolite and activated carbon) was estimated based on NREL calculation<sup>65</sup>. The membrane permeable  
276 to H<sub>2</sub> was modeled with the cape-open model called “MEMSIC” developed in our laboratory<sup>66</sup>.

277 The optimal design of the hybrid H<sub>2</sub> separation unit was determined based on the specific separation  
278 cost. The method used for the determination of the optimal architecture (membrane surface, pressure  
279 on the retentate and permeate of the membrane) is described in SI S7. The goal was to achieve  
280 99.99%vol hydrogen purity of hydrogen provided at 70 bar.

### 281 **2.2.9. Heat generation**

282 The tail gas of the hydrogen separation unit still contains some H<sub>2</sub>, CO, CH<sub>4</sub> and C<sub>2</sub>. Its lower heating  
283 value was too low for using it in an internal combustion engine for electricity production. Therefore,  
284 this gas was burnt in a gas boiler to produce heat for a heating network. The temperature range of the  
285 water network was 40/80°C.

286 The gas boiler model was adapted from François et al.<sup>27</sup>. We have implemented a Fortran subroutine  
287 fixing the pollutants yields based on the exhaust gas concentration of an industrial gas boiler. The  
288 atomic mass balance was computed with the same procedure as for the gasifier model.

### 289 **2.2.10. Thermal integration**

290 A pinch analysis was performed to build the heat exchanger network. The steam required for  
291 gasification was obtained with heat exchangers cooling the syngas before the reformer and the water-  
292 gas shift (case 1) or before the wet scrubber (case 2). The excess of heat was recovered for the heating  
293 network. Syngas and hydrogen compression requires multistage compression with intercooler. A part  
294 of this heat was used for preheating steam flow to feed the gasifier and the steam reformer, another  
295 part was recovered for the heat network. A small amount of cold water (15°C) was required as cooling  
296 utility to reach the lowest temperatures level in the process (30°C, between two compression stages).

297

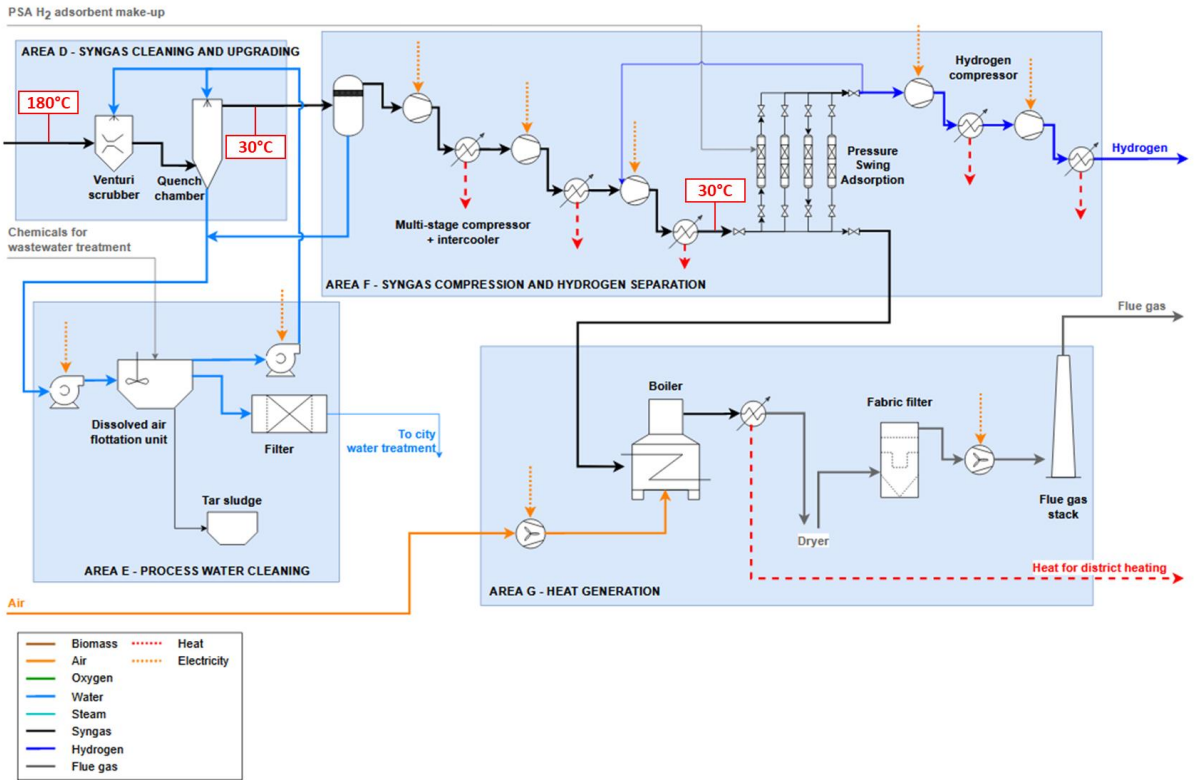
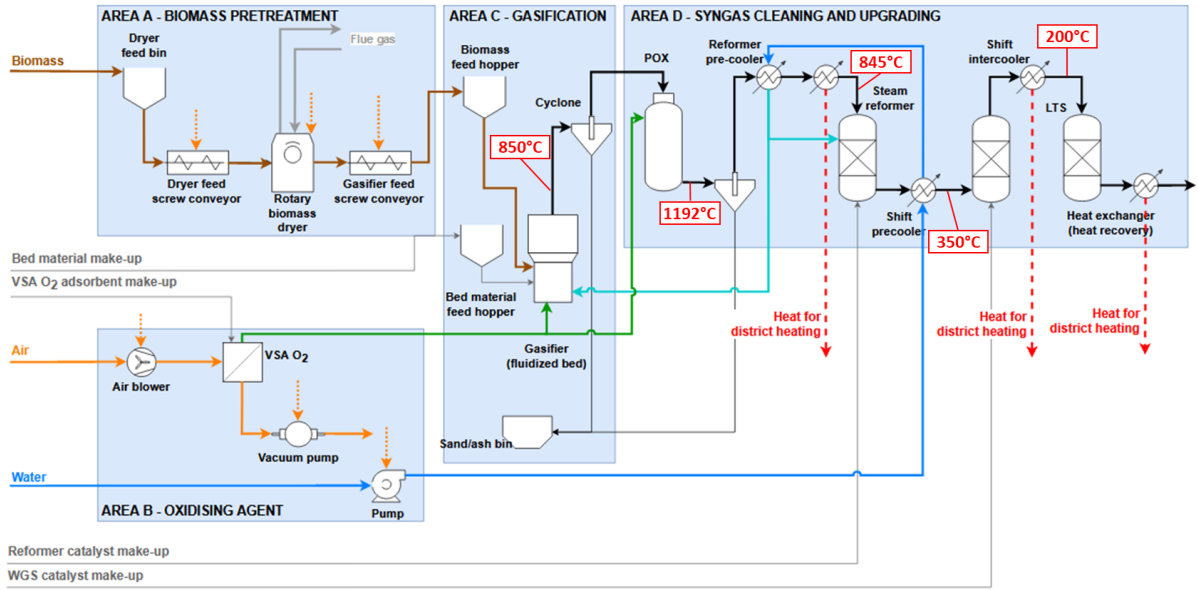


Figure 2: Detailed flow diagram of case 1.

**Table 2: Assumptions of the Aspen Plus model, utilities and material consumption.**

Unit	Methods	Results
Drier <sup>b</sup>	Adapted from François et al. <sup>27</sup>	Heat required, VOCs emissions
VSA O <sub>2</sub> <sup>a,c</sup>	SEP, O <sub>2</sub> recovery rate 55%	Air input
Gasifier <sup>d</sup>	RYIELD with external Fortran subroutine (experimental data <sup>17</sup> and atoms balances)	Composition of the syngas, temperature reached
Auto-thermal pyrolyser	RYIELD with external Fortran subroutine (ChemkinPro)	Composition of the syngas and bio-char, temperature reached
Cyclone	SEP, $\Delta P = 0.5$ kPa	
POX	Fortran subroutine, CHEMKIN-PRO simulation with adiabatic plug-flow reactor and radical kinetic mechanism <sup>57-59</sup>	Composition of the syngas after POX unit, temperature reached
Steam reformer <sup>e</sup>	RPLUG, kinetics in SI S6, $T_{inlet} = 845^{\circ}\text{C}$	Composition and temperature of the syngas after reformer, amount of catalyst.
Water-gas-shift <sup>f</sup>	RGIBBS, temperature approach $20^{\circ}\text{C}$ , $\Delta P = 0.4$ kPa, HTS ( $T_{inlet} = 350^{\circ}\text{C}$ ), LTS ( $T_{inlet} = 200^{\circ}\text{C}$ )	Composition and temperature of the syngas after WGS, amount of catalyst.
Water scrubber <sup>g</sup>	FLASH with experimental data, $\Delta P = 0.15$ kPa water flow rate adjusted to reach a syngas at $30^{\circ}\text{C}$ at the outlet.	Composition of the syngas after scrubber
Compressor <sup>a</sup>	Multi-stage compressor with intercooler ( $30^{\circ}\text{C}$ ), GPSA method, polytropic efficiency 0.80 and mechanical efficiency 0.98	Power required and outlet temperature.
Membrane H <sub>2</sub> <sup>i</sup>	Cape-open MEMSIC <sup>66</sup> , countercurrent flow pattern and permeance for UBE B-H membrane from <sup>67</sup> .	Compositions of the outlets and the corresponding membrane surface area
PSA H <sub>2</sub> <sup>h</sup>	SEP, recovery efficiency 85%, $\Delta P = 5$ kPa	Flow of hydrogen produced, composition of the tail gas, amount of adsorbent.
Air booster <sup>a</sup>	GPSA method, polytropic efficiency 0.80 and mechanical efficiency 0.98	Power required and outlet temperature.
Gas boiler	RYIELD with external Fortran subroutine adapted from François et al. <sup>27</sup> - excess of air $\lambda=1.5$ - CO: $0.006 \text{ kg/Nm}^3$ - C <sub>10</sub> H <sub>8</sub> : $4 \cdot 10^{-9} \text{ kg/Nm}^3$ - Other PAHs: $1.5 \cdot 10^{-9} \text{ kg/Nm}^3$ (acenaphthylene, anthracene, phenanthrene, pyrene) mole fraction 0.25 each. - NO mass fraction from oxidation of atmospheric N <sub>2</sub> $7 \cdot 10^{-5}$ - Soot $3 \cdot 10^{-5} \text{ kg/Nm}^3$ - VOC $0.25 \text{ g/Nm}^3$	Heat generated by the boiler, exhaust gas composition.
Heat exchanger	$\Delta P = 2$ kPa, minimum temperature approach $5^{\circ}\text{C}$	Surface area

<sup>a</sup>Estimated from Aspen Plus model assuming 80% polytropic efficiency and 98% mechanical efficiency for compressors and boosters.

<sup>b</sup>Ref<sup>20</sup> is used for conveyor and dryer consumption.

<sup>c</sup>Mass of fresh adsorbent per year estimated from Peters et al. and Swanson et al.<sup>19,68</sup>, adsorption isotherms for lithium doped adsorbent<sup>53</sup> assuming a 1-year lifetime (7500 hours of operations).

<sup>d</sup>Assuming 2.6 kg/h of fresh bed material for a 20 MW gasifier.

<sup>e</sup>Assuming SV 14 000 h<sup>-1</sup> and density 1025 kg/m<sup>3</sup><sup>24</sup>, catalyst replacement 33% per year.

<sup>f</sup>Assuming SV 2 700 h<sup>-1</sup> for HTS (iron and chromium oxide BASF K6-11 in<sup>10</sup>) and SV 5100 h<sup>-1</sup> for LTS (Cu/ZnO/Al<sub>2</sub>O<sub>3</sub> BASF K3-110 in<sup>11</sup>) and catalyst density 897.0 kg/m<sup>3</sup>, catalyst replacement 33% per year.

<sup>g</sup>Chemicals required for Dissolve Air Flotation unit and activated carbon guard bed for residual tars. Amount of activated carbon estimated assuming 3.25g PAH adsorbed per g of activated carbon<sup>62</sup>.

<sup>h</sup>Mass of fresh adsorbent per year estimated from Peters et al. and Swanson et al.<sup>19,68</sup>, adsorption isotherms for activated carbon and zeolite adsorbent<sup>65</sup> assuming a 4-year lifetime (7500 hours of operations).

<sup>i</sup>Since membrane module lifetime is expected to last 5 years, it assumed 20% of membrane surface replacement per year.

304

### 305 2.3. Definition of energetic efficiency

306 The energetic efficiency is defined with reference to the lower heating value of woodchips on dry basis.

307 The net  $\eta_{net}$  and gross  $\eta_{gross}$  energetic efficiencies are linked to heat  $\eta_{hn}$ , hydrogen  $\eta_{H_2}$  and bio-char

308  $\eta_{biochar}$  efficiency.

$$\eta_{net} = \eta_{hn} + \eta_{H_2} + \eta_{biochar} - \eta_{power\ consumption} \quad (1)$$

$$\eta_{gross} = \eta_{hn} + \eta_{H_2} + \eta_{biochar} \quad (2)$$

$$\eta_{hn} = \frac{\dot{Q}_{hn}}{\dot{m}_{wood,dry} \cdot LHV_{wood,dry}} \quad (3)$$

$$\eta_{H_2} = \frac{\dot{m}_{H_2} \cdot LHV_{H_2}}{\dot{m}_{wood,dry} \cdot LHV_{wood,dry}} \quad (4)$$

$$\eta_{biochar} = \frac{\dot{m}_{biochar} \cdot LHV_{biochar,dry}}{\dot{m}_{wood,dry} \cdot LHV_{wood,dry}} \quad (5)$$

$$\eta_{power\ consumption} = \frac{\dot{W}_{consumption}}{\dot{m}_{wood,dry} \cdot LHV_{wood,dry}} \quad (6)$$

309  $\dot{Q}_{hn}$  is the heat power sent to the heat network,  $\dot{m}_{wood,dry}$ ,  $\dot{m}_{H_2}$  and  $\dot{m}_{biochar}$  the mass flowrate of  
310 biomass, hydrogen and biochar.  $\dot{W}_{consumption}$  is the electrical power consumption.  $LHV_{biochar,dry}$   
311 and  $LHV_{wood,dry}$  are the lower heating value of biochar and wood.

### 312 3. RESULTS AND DISCUSSION

#### 313 3.1. Energy & Mass balance

314 The energy balances of each option are presented in Figure 3. The mass balance and the detailed  
315 composition of the main streams are available in SI S1. The main utilities consumptions including  
316 catalysts and adsorbents (Activated carbon AC and zeolite Ze) are given in Table 3. The electricity  
317 consumption was mainly driven by the hydrogen separation step and its compressors. The first option  
318 was the most electricity consuming because the entire syngas was compressed to 25 bar whereas the  
319 first stage of separation in cases 2 and 3 required a lower pressure (5 bar) (see supporting information  
320 S7). The electricity demand was also higher because of the final compression of H<sub>2</sub> on a bigger flow  
321 rate. The estimated amount of activated carbon to clean the excess water of residual PAHs and other  
322 contaminants was lower in the case 1 since the steam reformer reactor exhibits a catalytic effect on  
323 the tar reduction. The worst case for activated carbon consumption was the third case due to a higher  
324 quantity of tars in the syngas before wet scrubbing.

325 Spath et al. studied a similar process with indirectly heated biomass gasifier on a larger scale (434 MW  
326 LHV-basis). They determined a gross efficiency of 49.8% and a net efficiency of 45.6% for the  
327 production of hydrogen<sup>20</sup>. We found in this work a higher H<sub>2</sub> efficiency (57.6% gross and 52.0% net in  
328 case 1). This is mainly due to a better conversion of biomass into H<sub>2</sub> and CO in our case. At the exit of  
329 the gasifier, the yields were 24.8 mol<sub>H<sub>2</sub></sub>/kg<sub>biomass dry</sub> and 11.7 mol<sub>CO</sub>/kg<sub>biomass dry</sub> (O<sub>2</sub>/H<sub>2</sub>O bubbling  
330 fluidized bed<sup>17</sup>) compared to 8.4 mol<sub>H<sub>2</sub></sub>/kg<sub>biomass dry</sub> and 14.8 mol<sub>CO</sub>/kg<sub>biomass dry</sub> in Spath et al.<sup>20</sup>  
331 (a dual fluidized bed).

332 The second case without catalytic reactors gives a similar global efficiency (77.8% net) but the  
333 production of heat was higher (60.0% instead of 23.4%) and the production of H<sub>2</sub> smaller (17.9%  
334 instead of 52.0%). The second case is less interesting based on H<sub>2</sub> production, but its CAPEX and OPEX  
335 are probably significantly lower (two catalytic reactors were removed). Furthermore, this process can  
336 present an interest for the co-production of H<sub>2</sub> and heat for sites with higher heat demands.

337 The third case of autothermal pyrolysis and its three products (hydrogen, heat and bio-char) gives a  
338 higher efficiency (80.4% net) when the bio-char is considered as an energy product. The two energy  
339 vectors (hydrogen and heat) represent a 51.2% net efficiency. A large amount of syngas was recycled  
340 to the pyrolyser to maintain its fluidization.

341 In the autothermal pyrolysis option (case 3), 408 kg/h of bio-char are produced corresponding to a  
342 char yield around 11.0%daf and a carbon yield of 16.6%. This bio-char yield should be considered with  
343 caution because it is estimated from Ranzi's model of biomass pyrolysis and not validated in a pilot

344 plant. Yet, this model gives a rough estimate of the bio-char composition and the gas and tar detailed  
 345 composition. As a comparison, Polin et al. conducted autothermal pyrolysis at 500°C in a fluidized bed  
 346 of two biomasses: Red Oak and corn stover with an ER of 0.10 and 0.068, respectively. The biochar  
 347 yields were 9.5%wt for Red Oak and 20.1%wt for corn stover. The corresponding carbon yields were  
 348 estimated to 14.5% for Red Oak and 26.7% for corn stover<sup>69,70</sup>. The Red Oak experiments are compared  
 349 with the results of this model in SI 3. The model predicts nicely the overall permanent gas mass yield  
 350 but over-predicts the char yield (see SI 3 for more details).

351

**Table 3: Utilities consumption.**

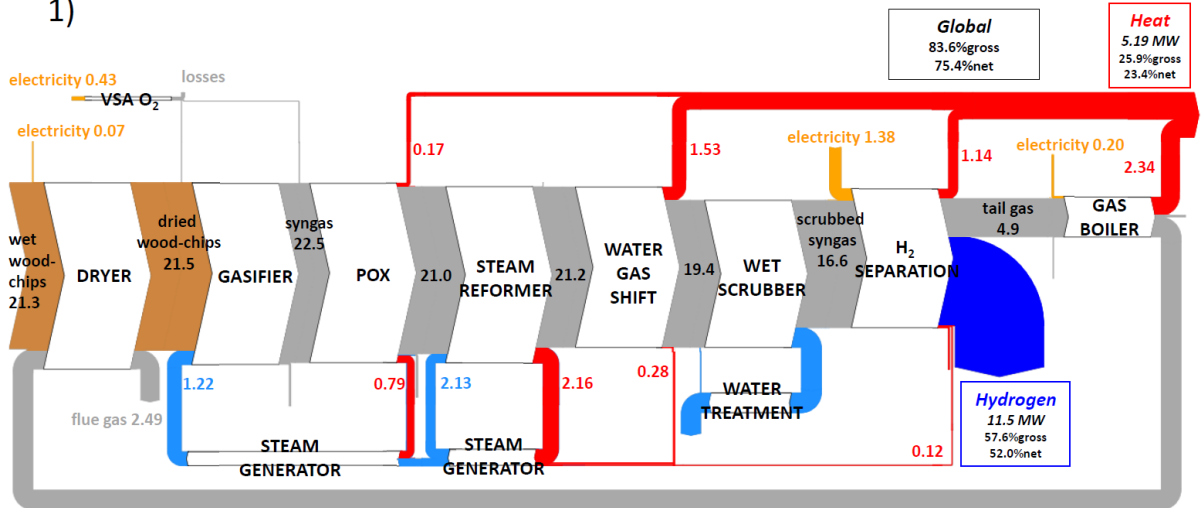
	Case 1	Case 2	Case 3
Electrical consumption [MWe]	2.08	1.66	1.36
Fresh water for steam generation [thousands of m <sup>3</sup> /y]	25.9	9.4	0
Adsorbent VSA O <sub>2</sub> [t/y]	0.96	0.96	0.63
Bed material [t/y]	19.5	19.5	19.5
Reformer catalyst [t/y]	0.25		
WGS catalyst [t/y]	HTS: 1.26 LTS: 0.68		
Chemicals for water treatment	NaOH: 210 t/y Flocculant: 23 m <sup>3</sup> /y Coagulant: 23 m <sup>3</sup> /y AC: 0.37 t/y	NaOH: 210 t/y Flocculant: 23 m <sup>3</sup> /y Coagulant: 23 m <sup>3</sup> /y AC: 11.7 t/y	NaOH: 210 t/y Flocculant: 23 m <sup>3</sup> /y Coagulant: 23 m <sup>3</sup> /y AC: 24.8 t/y
Adsorbent PSA H <sub>2</sub> [t/y]	AC: 0.465 Ze: 0.371	AC: 0.090 Ze: 0.071	AC: 0.063 Ze: 0.049
Membrane H <sub>2</sub> area [m <sup>2</sup> /y]		300	300
Natural gas <sup>a</sup> [Nm <sup>3</sup> /y]	3600	3600	3600
Nitrogen <sup>b</sup> [Nm <sup>3</sup> /y]	3600	3600	3600

<sup>a</sup>Estimate for two start-ups per year and auxiliary fuel for flare.

<sup>b</sup>Estimate for the nitrogen safety system.

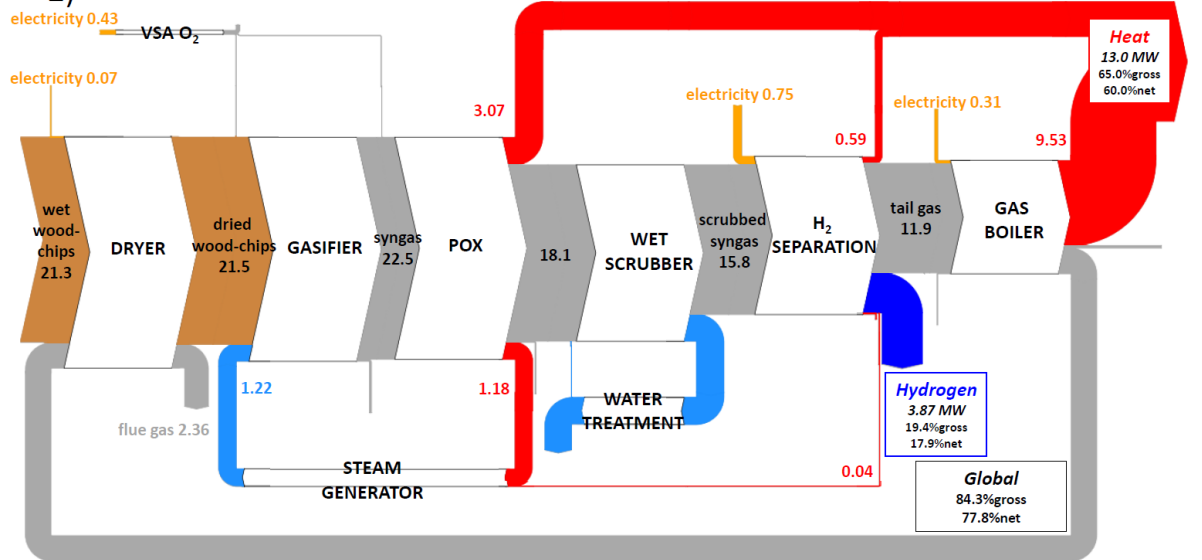
352

1)



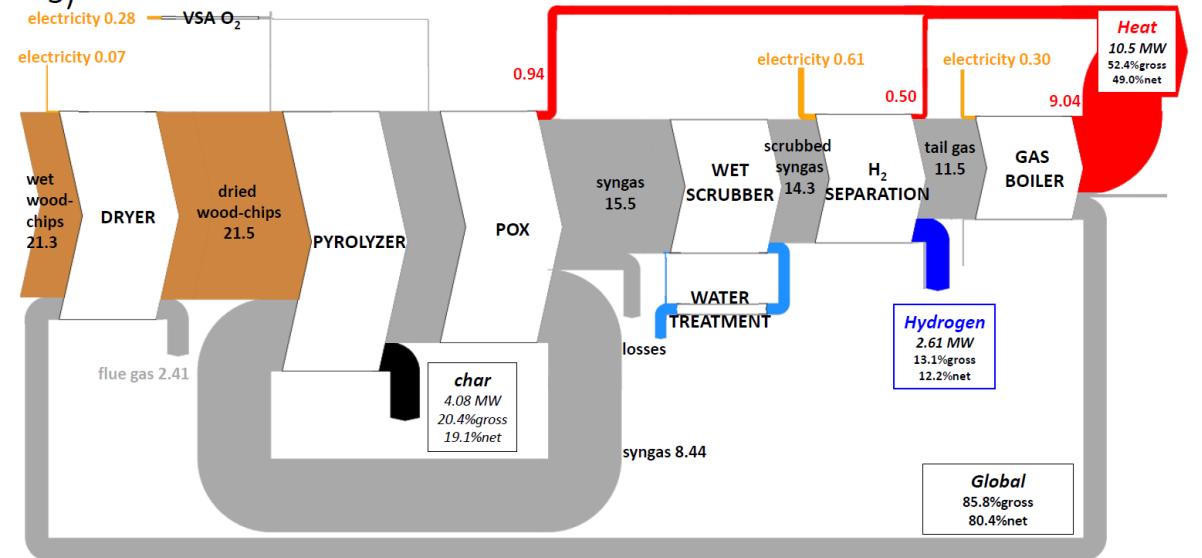
353

2)



354

3)



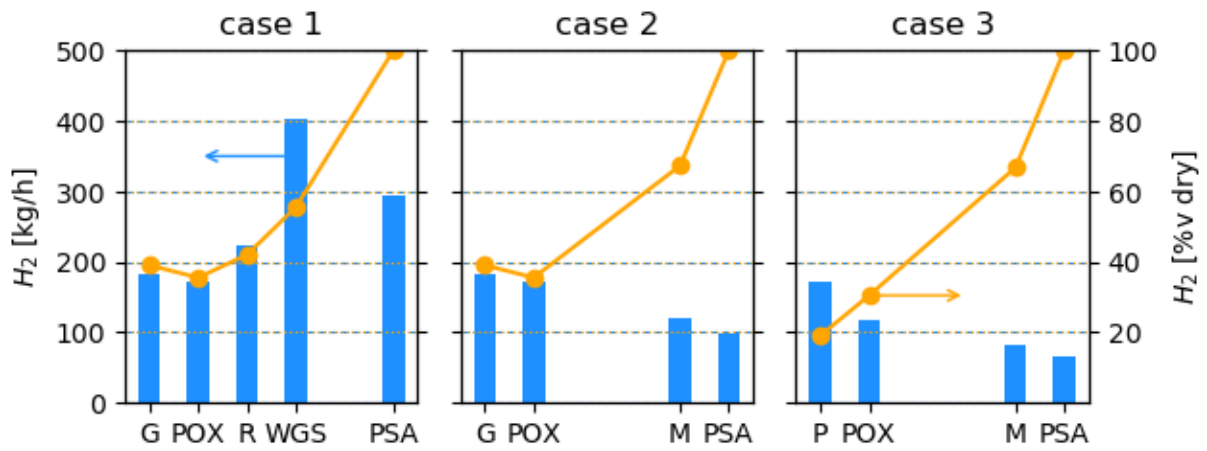
355

356

Figure 3: Sankey's type diagrams (in MW) of the 3 cases.

357 **3.2. Fate of hydrogen along the process unit**

358 Figure 4 shows the molar flow rate and fraction of hydrogen along the process for each option.



359

360 **Figure 4: Hydrogen molar flow rate and fraction along the process. G=Gasifier, P=Pyrolyzer,**  
 361 **POX=Partial Oxidation, R=Reformer, WGS=Water Gas Shift, M=Membrane, PSA=Pressure Swing**  
 362 **Adsorption.**

363 The objective was to reach 70%vol of H<sub>2</sub> before the PSA to produce quasi-pure hydrogen with the PSA  
 364 H<sub>2</sub>. The flow rate of hydrogen is doubled when catalytic reformer and water-gas-shift reactors are used  
 365 (Figure 4). Its molar fraction is increased from 35.5% to 55.5%db. This concentration is reached in case  
 366 2 and 3 with a membrane module (67.3 and 66.8%db respectively for cases 2 and 3). The 70%vol  
 367 concentration is achieved by recirculating a part of the hydrogen produced.

368 In the best case (1), 107 g<sub>H<sub>2</sub></sub>/kg<sub>biomass,dry</sub> could be produced in which 79 g are effectively separated  
 369 (76% recovery). This result compares well with the 140 g<sub>H<sub>2</sub></sub>/kg<sub>biomass,dry</sub> produced claimed by Corella  
 370 et al.<sup>11</sup> for oxy-steam gasification followed by reformer and shift reactors. This lower yield of hydrogen  
 371 can be explained by the partial oxidation of a part of the hydrogen in the POX unit. This reactor is  
 372 necessary because the syngas produced by Schmid et al.<sup>17</sup> contains more tars than Corella et al.<sup>11</sup> with  
 373 dolomite as bed material. Indeed the syngas produced by Corella et al. contains less than 2 g/Nm<sup>3</sup> of  
 374 tars whereas, the syngas produced by Schmid et al. contains 38 g/Nm<sup>3</sup><sup>17</sup>.

375 When catalytic reactors are removed, the hydrogen production is divided by a factor of 2 or 3. In case  
 376 2, 47 g<sub>H<sub>2</sub></sub>/kg<sub>biomass,dry</sub> could be produced in which 26 g are effectively separated. In the case 3,  
 377 31 g<sub>H<sub>2</sub></sub>/kg<sub>biomass,dry</sub> could be produced and 18 g are separated. These two cases present smaller  
 378 hydrogen production but they could be more suitable for a territorial level: the processes are simpler  
 379 and more robust than with catalytic reactors. The separation process of hydrogen was chosen to  
 380 minimize the hydrogen specific separation cost but this architecture did not lead necessarily to the

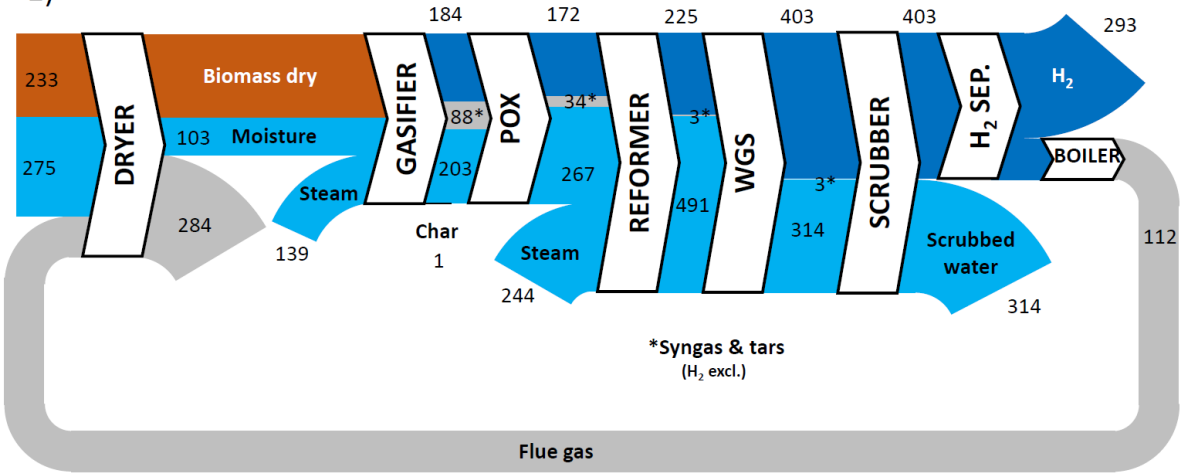
381 maximum hydrogen recovery rate. A higher production of H<sub>2</sub> would lead to higher specific separation  
382 cost. In case 3, char is produced and may be used to create a carbon sink.

383 The final H<sub>2</sub> yield of case 1 (79 g<sub>H<sub>2</sub></sub>/kg<sub>biomass,dry</sub>) is in good agreement with previous studies. In  
384 bubbling fluidized bed, Ersöz et al. evaluated a yield of 76.1 g<sub>H<sub>2</sub></sub>/kg<sub>biomass,dry</sub> after PSA<sup>36</sup>. Susmozas  
385 et al. found a lower value in a steam dual fluidized bed: 55.0 g<sub>H<sub>2</sub></sub>/kg<sub>biomass,dry</sub><sup>41</sup> whereas Pallozzi et  
386 al. found 75.2 g<sub>H<sub>2</sub></sub>/kg<sub>biomass,dry</sub><sup>42</sup> for the same technology. Gupta and Dasappa determined  
387 107.4 g<sub>H<sub>2</sub></sub>/kg<sub>biomass,dry</sub><sup>37</sup> with a fixed bed downdraft. The values obtained for case 2 and 3 of this  
388 study cannot be compared because our separation process had never been previously proposed.

389 In order to better understand the H atoms transfer from wood and water to H<sub>2</sub>, Figure 5 shows the  
390 fate of H along the process units. In the first scenario, 42.7% of the produced H<sub>2</sub> comes from the oxy-  
391 steam gasification of biomass after the POX unit, 13.2% results from steam reforming and 44.2% from  
392 water gas-shift reactors. As a consequence of catalytic reactors, almost all the hydrogen content in the  
393 syngas before the separation process is attributed to the H<sub>2</sub> molecule. In the second case, all the H<sub>2</sub>  
394 comes from biomass and steam during gasification. As in case 1, after the partial oxidation of the  
395 syngas to reduce the amount of tars, the hydrogen yield was slightly reduced by 6%. The temperature  
396 in the POX unit was too high to promote the conversion of CO by the water gas-shift. In the third case,  
397 the POX unit increases the hydrogen yield from 19.4%v after pyrolysis to 31%v on a dry basis. The H<sub>2</sub>  
398 content in case 3 is lower than in case 2. First, a part of hydrogen is kept in bio-char. In addition, the  
399 carbon in biochar which is not converted into syngas as CO could not contribute to the H<sub>2</sub> formation  
400 by the water-gas shift reaction. To increase the amount of hydrogen after POX unit, we tried to add  
401 steam in the POX. This addition has no effect on H<sub>2</sub> formation. Indeed, as shown by our group<sup>71</sup>, OH  
402 radicals mainly result from CO<sub>2</sub> conversion during syngas thermal conversion and H<sub>2</sub>O is poorly reactive  
403 under such conditions.

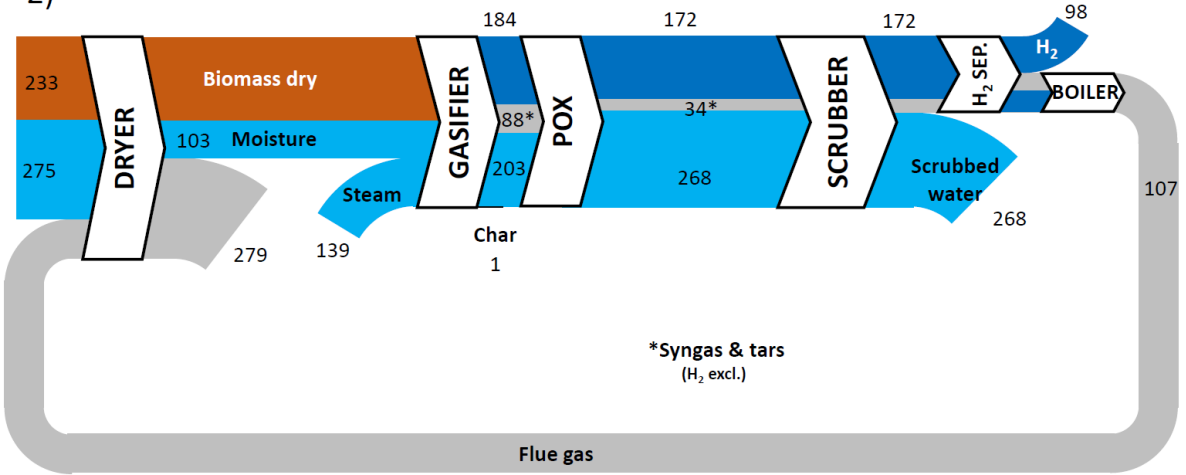
404

1)



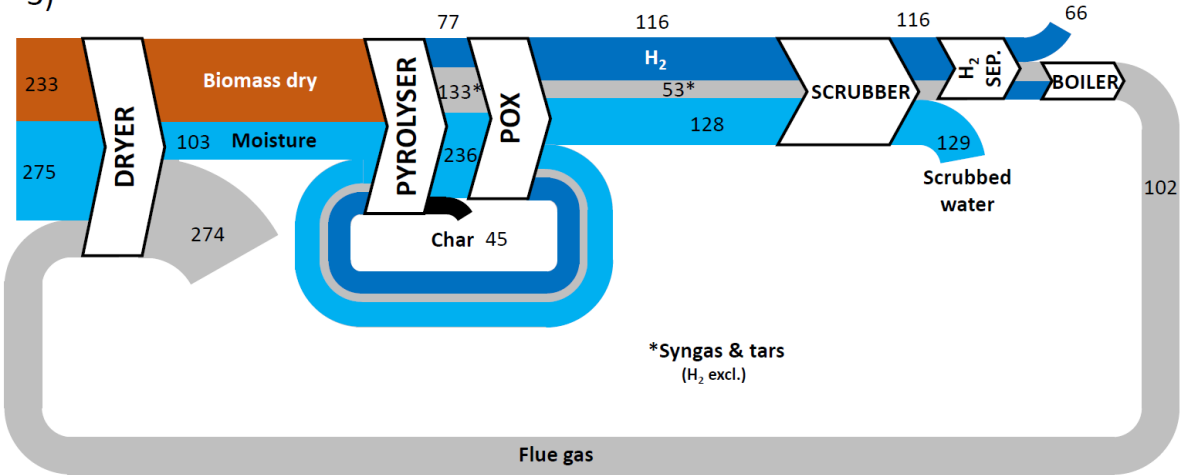
405

2)



406

3)



407

408

Figure 5: Fate of atomic hydrogen along the process for each scenario (kg<sub>H</sub>/h).

409

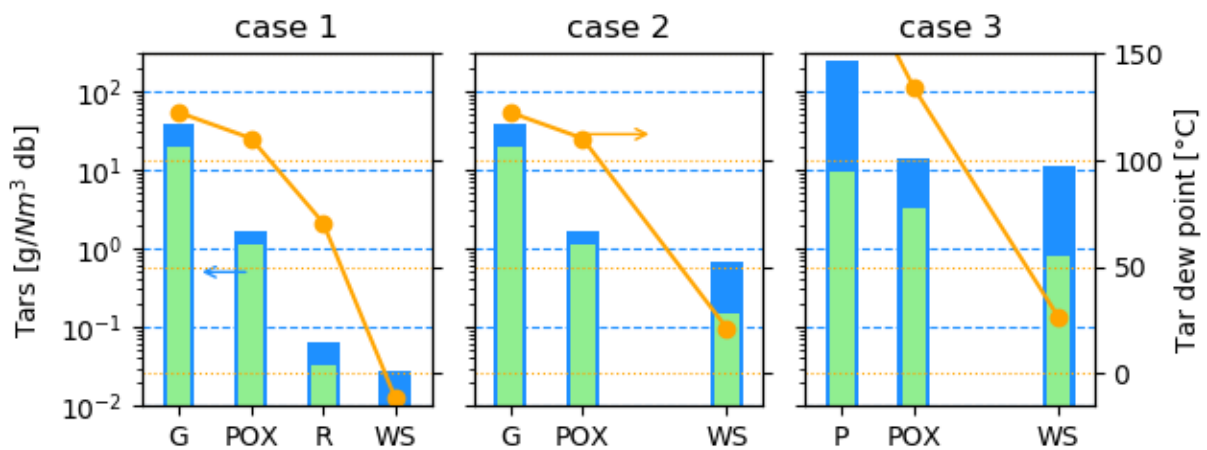
410

411 **3.3. Tar and particles**

412 The Figure 6 shows the tar dew point and the tar concentration in the syngas along the process. The  
 413 POX unit seems to have no effect on tar dew point. In fact, tars are effectively converted but the  
 414 heaviest tars mainly control the dew point value even at very low concentration. A higher amount of  
 415 oxygen would increase the efficiency of the POX unit. Unfortunately, the temperature rise would have  
 416 been too high for the refractory material of the reactor. The addition of oxygen was then limited by  
 417 the temperature reached in the POX unit (Figure 7) (more details presented in SI S5). The temperature  
 418 limit was set to 1300°C for a classical refractory material of the POX unit. The peak temperature  
 419 corresponds to the maximum temperature reached in the POX unit.

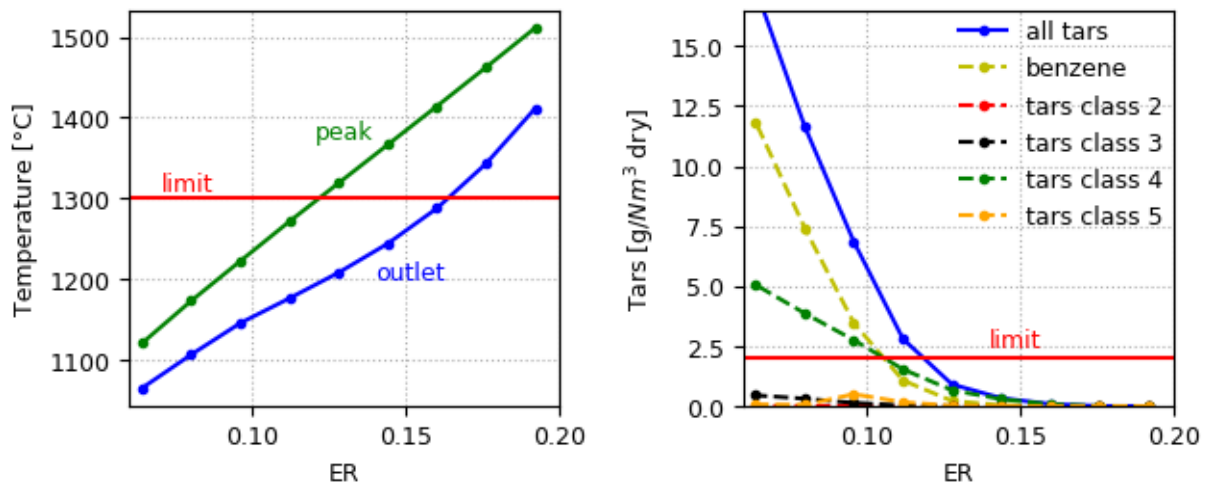
420 The reduction of global tar concentration is relatively small after the wet scrubber for case 1, but this  
 421 equipment is required for water condensation from syngas. It also plays the role of extra dust/soot  
 422 removal. The heaviest PAHs are removed by the wet scrubber, thus reducing the tar dew point.

423 In case 3, the POX unit is not able to reduce the amount of tars below 2 g/Nm<sup>3</sup> as for gasification  
 424 scenarios, even with higher gas-phase residence times. The addition of oxygen was limited by the  
 425 temperature reached (max 1300°C). The initial content of tars is higher after pyrolysis than after  
 426 gasification. Its composition is also different with more primary and secondary tars. However, the tar  
 427 dew point is reduced to around 25°C after the wet scrubber.



428

429 **Figure 6: Concentration of tars and tar dew point along the process. G=Gasifier, P=Pyrolyzer,**  
 430 **POX=Partial Oxidation, R=Reformer, WS=Water Scrubber. Tars and benzene in blue, tars without**  
 431 **benzene in green.**



432

433 **Figure 7: Impact of ER on POX temperature and reduction of tars (for cases 1 and 2).**

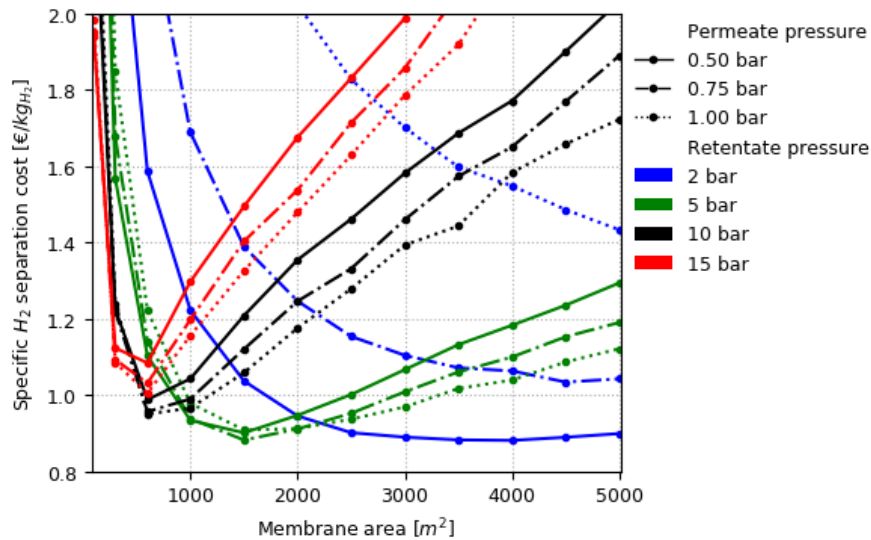
434

435 **3.4. H<sub>2</sub> separation by a hybrid process: membrane coupled to PSA**

436 Two stages of separation were required (membrane and PSA) when the H<sub>2</sub> concentration in the syngas  
 437 was too low, since a single PSA would require a very large product recycling to reach 70%v at the inlet<sup>20</sup>.  
 438 The membrane as a first stage plays the role of a pre-concentrator before the PSA (see supplementary  
 439 material S7). To the best of our knowledge, this architecture of hydrogen separation from a biomass  
 440 syngas is proposed for the first time. No data is available on the membrane lifetime using syngas with  
 441 a residual amount of tars. If necessary, a guard bed filled with activated carbon could be added to  
 442 remove these tars before the separation stage.

443 The minimum specific separation costs were estimated at 0.91 and 1.08 €/kg<sub>H<sub>2</sub></sub> for case 2 (Figure 8)  
 444 and 3 respectively (SI S7). The first stage of separation with the membrane module requires a syngas  
 445 pressure of around 5 bar, which is lower than the pressure required for PSA H<sub>2</sub> (around 25 bar). Only  
 446 a part of the syngas enriched in hydrogen is compressed to this higher pressure in the second stage.  
 447 As a result, the required energy is lowered with these two levels of pressure. The operational  
 448 expenditure is decreased for the power consumption, but the H<sub>2</sub> recovery rate is lower. This explains  
 449 why the specific separation cost is only 0.59 €/kg<sub>H<sub>2</sub></sub> in the case 1 with one stage PSA.

450



451

452 **Figure 8: Specific hydrogen separation cost for case 2 as a function of membrane area, permeate**  
 453 **and retentate pressures.**

454

455 **3.5. Comparison of the various options and recommendations**

456 The choice between these scenarios is dependent on various criteria. The heat represents roughly  
 457 between one third and more than half of energy outputs. Therefore, the choice may depend on the  
 458 valorization of heat on the selected locations (like industrial sites). In any case, it would be far better if  
 459 the heat demand of the site is relatively constant during the year. The availability of the feedstock is  
 460 another criterion on the scale that is linked to the location of the plant. Finally, this location should  
 461 avoid the transport of hydrogen on large distance by trucks. The bio-char can be more easily  
 462 transported than hydrogen, but its production supposes a demand nearby since its density is quite  
 463 low. This bio-char could also be stored or sequestered to create a carbon sink<sup>3</sup>.

464 Case 1 could fulfill hydrogen demand at 293 kg<sub>H2</sub>/h and it produces 5.2 MW<sub>th</sub> of heat that must be  
 465 valorized. Case 2 and 3 are simpler from a technology point of view: fewer unit operations, no catalytic  
 466 reactor. This gain in robustness has to be counterbalanced with the hydrogen separation process that  
 467 is more complex. The production of hydrogen is also far lower 98 kg<sub>H2</sub>/h in case 2 and only 66 kg<sub>H2</sub>/h  
 468 in case 3.

469 From these results, we could expect the capital costs of case 1 to be much higher than cases 2 and 3  
 470 due to the catalytic reactors and the additional cost of catalysts. However, for cases 2 and 3, the  
 471 hydrogen separation was achieved in two stages, increasing the specific cost of hydrogen separation.  
 472 This point should be quantified properly with a further techno-economic assessment.

473 The third case can be chosen for its carbon sequestration potential through bio-char production. This  
474 option leads to a net negative CO<sub>2</sub> emission process as it may lead to a stable sink of carbon<sup>3</sup>.

475 Furthermore, in the context of bioenergy with carbon capture and storage (BECCS) processes, the PSA  
476 tail gas has a high concentration of CO<sub>2</sub> (between 60 to 70%v according to the cases). This high  
477 concentration favors the capture of CO<sub>2</sub> for carbon sequestration.

478

#### 479 **4. CONCLUSION**

480 The aim of this work was to provide a detailed mass and energy balance of three scenarios of  
481 production of hydrogen from biomass: a first case dedicated to produce the maximum of hydrogen, a  
482 simpler option without catalyst reactors and a carbon-negative process that also produced bio-char.

483 The model covered the whole process from drying of the biomass to the production of H<sub>2</sub>, heat and  
484 bio-char. All these operation units were modeled with Aspen Plus® with a detailed composition of tars.  
485 The accuracy of the model was ensured with experimental data when they were available. Chemkin  
486 Pro was coupled to Aspen Plus® to model the partial oxidation unit with a detailed radical kinetic  
487 mechanism. A hybrid hydrogen separation process was proposed using two technologies, namely  
488 membrane and PSA. The high-temperature heat was recovered for steam generation used for the  
489 gasification. The low-grade heat was used for woodchips drying whereas the rest of the heat was  
490 valorized in a heating network.

491 Global energetic efficiencies are 75.4, 77.8 and 80.4%net for scenarios 1 to 3, respectively. The  
492 hydrogen yields were 79, 26 and 18 g<sub>H<sub>2</sub></sub>/kg<sub>biomass,dry</sub> after separation. The excess of heat dedicated  
493 to a heating network leads to heat efficiencies of 23.4, 60.0 and 49.0%net for the same three options  
494 respectively. 110 g<sub>biochar</sub>/kg<sub>biomass,dry</sub> was produced in the third option. The needs of utilities and  
495 commodities are also quantified.

496 These data will be used in a techno-economic assessment and a life cycle assessment to consider all  
497 the aspects: profitability and environmental impacts.

498 The production of renewable hydrogen from biomass represents an alternative path to electrolysis  
499 processes when the available electricity production is too low or too carbon intensive.

500

#### 501 **5. SUPPORTING INFORMATIONS**

502 The supporting information file 1 presents: 1) details flowsheets of each scenarios and mass balance  
503 results, 2) the composition of the syngas and tars used as experimental data for oxy-steam gasification,  
504 3) the presentation and the results of the auto-thermal pyrolyser model, 4) few details about the  
505 partial oxidation model, 5) the influence of the equivalent ratio on the efficiency of the partial  
506 oxidation unit, 6) the kinetic model used for the steam reformer model, 7) the methods and results  
507 used to define the architecture of the hydrogen separation. The supporting information file 2 presents  
508 the detailed composition of each flow from Aspen Plus.

509

## 510 6. FUNDINGS

511 This work was funded by the French PIA project “Lorraine Université d’Excellence” (reference ANR-15-  
512 IDEX-04-LUE) and by the Hy-C-GREEN project (Europe-FEDER and Grand-Est province).

513

## 514 7. REFERENCES

- 515 (1) Smil, V. *Energy Transitions: Global and National Perspectives*, Second edition.; Praeger, an  
516 imprint of ABC-CLIO, LLC: Santa Barbara, California Denver, Colorado, 2017.
- 517 (2) *Bp Statistical Review of World Energy 2021*; 2021.
- 518 (3) Dufour, A. Geological Sequestration of Biomass Char to Mitigate Climate Change. *Environmental  
519 Science & Technology* **2013**, 130829114030003. <https://doi.org/10.1021/es4036418>.
- 520 (4) Williams, R. H.; Larson, E. D.; Katofsky, R. E.; Chen, J. Methanol and Hydrogen from Biomass for  
521 Transportation. *Energy for Sustainable Development* **1995**, 1 (5), 18–34.  
522 [https://doi.org/10.1016/S0973-0826\(08\)60083-6](https://doi.org/10.1016/S0973-0826(08)60083-6).
- 523 (5) *The Future of Hydrogen*; IEA, 2019; p 203.
- 524 (6) Ministère de la Transition Énergétique et Solidaire. *Stratégie Française Pour l’énergie et Le  
525 Climat - Programmation Pluriannuelle de l’énergie 2019-2023 2024-2028*; 2018.
- 526 (7) Woolcock, P. J.; Brown, R. C. A Review of Cleaning Technologies for Biomass-Derived Syngas.  
527 *Biomass and Bioenergy* **2013**, 52, 54–84. <https://doi.org/10.1016/j.biombioe.2013.02.036>.
- 528 (8) Xu, G.; Murakami, T.; Suda, T.; Matsuzawa, Y.; Tani, H. The Superior Technical Choice for Dual  
529 Fluidized Bed Gasification. *Ind. Eng. Chem. Res.* **2006**, 45 (7), 2281–2286.  
530 <https://doi.org/10.1021/ie051099r>.
- 531 (9) Corella, J.; Toledo, J. M.; Molina, G. A Review on Dual Fluidized-Bed Biomass Gasifiers. *Industrial  
532 & Engineering Chemistry Research* **2007**, 46 (21), 6831–6839.  
533 <https://doi.org/10.1021/ie0705507>.
- 534 (10) Larsson, A.; Thunman, H.; Ström, H.; Sasic, S. Experimental and Numerical Investigation of the  
535 Dynamics of Loop Seals in a Large-Scale DFB System under Hot Conditions. *AIChE Journal* **2015**,  
536 61 (11), 3580–3593. <https://doi.org/10.1002/aic.14887>.
- 537 (11) Corella, J.; Aznar, M.; Caballero, M.; Molina, G.; Toledo, J. 140gH<sub>2</sub>/Kg Biomass d.a.f. by a CO-  
538 Shift Reactor Downstream from a FB Biomass Gasifier and a Catalytic Steam Reformer.  
539 *International Journal of Hydrogen Energy* **2008**, 33 (7), 1820–1826.  
540 <https://doi.org/10.1016/j.ijhydene.2008.02.003>.

- 541 (12) Bates, R. B.; Altantzis, C.; Ghoniem, A. F. Modeling of Biomass Char Gasification, Combustion,  
542 and Attrition Kinetics in Fluidized Beds. *Energy Fuels* **2016**, *30* (1), 360–376.  
543 <https://doi.org/10.1021/acs.energyfuels.5b02120>.
- 544 (13) Kersten, S. R. A.; Wang, X.; Prins, W.; van Swaaij, W. P. M. Biomass Pyrolysis in a Fluidized Bed  
545 Reactor. Part 1: Literature Review and Model Simulations. *Ind. Eng. Chem. Res.* **2005**, *44* (23),  
546 8773–8785. <https://doi.org/10.1021/ie0504856>.
- 547 (14) Bruchmüller, J.; van Wachem, B. G. M.; Gu, S.; Luo, K. H.; Brown, R. C. Modeling the  
548 Thermochemical Degradation of Biomass inside a Fast Pyrolysis Fluidized Bed Reactor. *AIChE*  
549 *Journal* **2012**, *58* (10), 3030–3042. <https://doi.org/10.1002/aic.13705>.
- 550 (15) Brown, R. C. Heterodoxy in Fast Pyrolysis of Biomass. *Energy Fuels* **2021**, *35* (2), 987–1010.  
551 <https://doi.org/10.1021/acs.energyfuels.0c03512>.
- 552 (16) Lehmann, J. A Handful of Carbon. *Nature* **2007**, *447* (7141), 143–144.  
553 <https://doi.org/10.1038/447143a>.
- 554 (17) Schmid, M.; Beirow, M.; Schweitzer, D.; Waizmann, G.; Spörl, R.; Scheffknecht, G. Product Gas  
555 Composition for Steam-Oxygen Fluidized Bed Gasification of Dried Sewage Sludge, Straw Pellets  
556 and Wood Pellets and the Influence of Limestone as Bed Material. *Biomass and Bioenergy* **2018**,  
557 *117*, 71–77. <https://doi.org/10.1016/j.biombioe.2018.07.011>.
- 558 (18) Barisano, D.; Canneto, G.; Nanna, F.; Alvino, E.; Pinto, G.; Villone, A.; Carnevale, M.; Valerio, V.;  
559 Battafarano, A.; Braccio, G. Steam/Oxygen Biomass Gasification at Pilot Scale in an Internally  
560 Circulating Bubbling Fluidized Bed Reactor. *Fuel Processing Technology* **2016**, *141*, 74–81.  
561 <https://doi.org/10.1016/j.fuproc.2015.06.008>.
- 562 (19) Swanson, R. M.; Platon, A.; Satrio, J. A.; Brown, R. C.; Hsu, D. D. *Techno-Economic Analysis of*  
563 *Biofuels Production Based on Gasification*; NREL/TP-6A20-46587, 994017; 2010.  
564 <https://doi.org/10.2172/994017>.
- 565 (20) Spath, P.; Aden, A.; Eggeman, T.; Ringer, M.; Wallace, B.; Jechura, J. *Biomass to Hydrogen*  
566 *Production Detailed Design and Economics Utilizing the Battelle Columbus Laboratory Indirectly-*  
567 *Heated Gasifier*; NREL/TP-510-37408, 15016221; 2005. <https://doi.org/10.2172/15016221>.
- 568 (21) Fail, S.; Diaz, N.; Benedikt, F.; Kraussler, M.; Hinteregger, J.; Bosch, K.; Hackel, M.; Rauch, R.;  
569 Hofbauer, H. Wood Gas Processing To Generate Pure Hydrogen Suitable for PEM Fuel Cells. *ACS*  
570 *Sustainable Chemistry & Engineering* **2014**, *2* (12), 2690–2698.  
571 <https://doi.org/10.1021/sc500436m>.
- 572 (22) Kraussler, M.; Binder, M.; Hofbauer, H. 2250-h Long Term Operation of a Water Gas Shift Pilot  
573 Plant Processing Tar-Rich Product Gas from an Industrial Scale Dual Fluidized Bed Biomass  
574 Steam Gasification Plant. *International Journal of Hydrogen Energy* **2016**, *41* (15), 6247–6258.  
575 <https://doi.org/10.1016/j.ijhydene.2016.02.137>.
- 576 (23) Hamelinck, C. N.; Faaij, A. P. C. Future Prospects for Production of Methanol and Hydrogen from  
577 Biomass. *Journal of Power Sources* **2002**, *22*.
- 578 (24) Caballero, M. A.; Aznar, M. P.; Gil, J.; Martín, J. A.; France, E. Commercial Steam Reforming  
579 Catalysts To Improve Biomass Gasification with Steam-Oxygen Mixtures. 1. Hot Gas Upgrading  
580 by the Catalytic Reactor. *Ind. Eng. Chem. Res.* **1997**, *36* (5227–5239).
- 581 (25) Aznar, M. P.; Caballero, M. A.; Gil, J.; Martín, J. A.; Corella, J. Commercial Steam Reforming  
582 Catalysts To Improve Biomass Gasification with Steam-Oxygen Mixtures. 2. Catalytic Tar  
583 Removal. *Industrial & Engineering Chemistry Research* **1998**, *37*, 2668–2680.
- 584 (26) Chianese, S.; Fail, S.; Binder, M.; Rauch, R.; Hofbauer, H.; Molino, A.; Blasi, A.; Musmarra, D.  
585 Experimental Investigations of Hydrogen Production from CO Catalytic Conversion of Tar Rich  
586 Syngas by Biomass Gasification. *Catalysis Today* **2016**, *277*, 182–191.  
587 <https://doi.org/10.1016/j.cattod.2016.04.005>.
- 588 (27) François, J.; Mauviel, G.; Feidt, M.; Rogaume, C.; Rogaume, Y.; Mirgaux, O.; Patisson, F.; Dufour,  
589 A. Modeling of a Biomass Gasification CHP Plant: Influence of Various Parameters on Energetic  
590 and Exergetic Efficiencies. *Energy & Fuels* **2013**, *27* (12), 7398–7412.  
591 <https://doi.org/10.1021/ef4011466>.

- 592 (28) Emonts, B.; Reuß, M.; Stenzel, P.; Welder, L.; Knicker, F.; Grube, T.; Görner, K.; Robinius, M.;  
593 Stolten, D. Flexible Sector Coupling with Hydrogen: A Climate-Friendly Fuel Supply for Road  
594 Transport. *International Journal of Hydrogen Energy* **2019**, *44* (12918–12930), 13.  
595 <https://doi.org/10.1016/j.ijhydene.2019.03.1>.
- 596 (29) Francois, J.; Abdelouahed, L.; Mauviel, G.; Patisson, F.; Mirgaux, O.; Rogaume, C.; Rogaume, Y.;  
597 Feidt, M.; Dufour, A. Detailed Process Modeling of a Wood Gasification Combined Heat and  
598 Power Plant. *Biomass and Bioenergy* **2013**, *51*, 68–82.  
599 <https://doi.org/10.1016/j.biombioe.2013.01.004>.
- 600 (30) Puig-Arnavat, M.; Bruno, J. C.; Coronas, A. Review and Analysis of Biomass Gasification Models.  
601 *Renewable and Sustainable Energy Reviews* **2010**, *14* (9), 2841–2851.  
602 <https://doi.org/10.1016/j.rser.2010.07.030>.
- 603 (31) Srinivas, S.; Field, R. P.; Herzog, H. J. Modeling Tar Handling Options in Biomass Gasification.  
604 *Energy Fuels* **2013**, *27* (6), 2859–2873. <https://doi.org/10.1021/ef400388u>.
- 605 (32) Abdelouahed, L.; Authier, O.; Mauviel, G.; Corriou, J. P.; Verdier, G.; Dufour, A. Detailed  
606 Modeling of Biomass Gasification in Dual Fluidized Bed Reactors under Aspen Plus. *Energy &*  
607 *Fuels* **2012**, *26* (6), 3840–3855. <https://doi.org/10.1021/ef300411k>.
- 608 (33) Gómez-Barea, A.; Leckner, B. Modeling of Biomass Gasification in Fluidized Bed. *Progress in*  
609 *Energy and Combustion Science* **2010**, *36* (4), 444–509.  
610 <https://doi.org/10.1016/j.pecs.2009.12.002>.
- 611 (34) Bates, R. B.; Ghoniem, A. F.; Jablonski, W. S.; Carpenter, D. L.; Altantzis, C.; Garg, A.; Barton, J.  
612 L.; Chen, R.; Field, R. P. Steam-Air Blown Bubbling Fluidized Bed Biomass Gasification (BFBBG):  
613 Multi-Scale Models and Experimental Validation. *AIChE Journal* **2017**, *63* (5), 1543–1565.  
614 <https://doi.org/10.1002/aic.15666>.
- 615 (35) Martín, M.; Grossmann, I. E. Process Optimization of FT-Diesel Production from Lignocellulosic  
616 Switchgrass. *Ind. Eng. Chem. Res.* **2011**, *50* (23), 13485–13499.  
617 <https://doi.org/10.1021/ie201261t>.
- 618 (36) Ersöz, A.; DurakÇetin, Y.; Sarioğlan, A.; Turan, A. Z.; Mert, M. S.; Yüksel, F.; Figen, H. E.; Güldal,  
619 N. Ö.; Karaismailoğlu, M.; Baykara, S. Z. Investigation of a Novel & Integrated Simulation Model  
620 for Hydrogen Production from Lignocellulosic Biomass. *International Journal of Hydrogen*  
621 *Energy* **2018**, *43* (2), 1081–1093. <https://doi.org/10.1016/j.ijhydene.2017.11.017>.
- 622 (37) Gupta, A.; Dasappa, S. Hydrogen from Biomass by Oxy-Steam Gasification - A Quantitative  
623 Analysis of Cases. *Proceedings of the 26th European Biomass Conference and Exhibition 2018*,  
624 *14-17 May 2018*, 4 Pages. <https://doi.org/10.5071/26THEUBCE2018-2CV.4.22>.
- 625 (38) Kalinci, Y.; Hepbasli, A.; Dincer, I. Exergoeconomic Analysis of Hydrogen Production from  
626 Biomass Gasification. *International Journal of Hydrogen Energy* **2012**, *37* (21), 16402–16411.  
627 <https://doi.org/10.1016/j.ijhydene.2012.02.173>.
- 628 (39) Ishaq, H.; Dincer, I. A Novel Biomass Gasification Based Cascaded Hydrogen and Ammonia  
629 Synthesis System Using Stoichiometric and Gibbs Reactors. *Biomass and Bioenergy* **2021**, *145*,  
630 105929. <https://doi.org/10.1016/j.biombioe.2020.105929>.
- 631 (40) Koroneos, C.; Dompros, A.; Roubas, G. Hydrogen Production via Biomass Gasification —A Life  
632 Cycle Assessment Approach. *Chemical Engineering and Processing: Process Intensification* **2008**,  
633 *47* (8), 1261–1268. <https://doi.org/10.1016/j.cep.2007.04.003>.
- 634 (41) Susmozas, A.; Iribarren, D.; Zapp, P.; Linßen, J.; Dufour, J. Life-Cycle Performance of Hydrogen  
635 Production via Indirect Biomass Gasification with CO<sub>2</sub> Capture. *International Journal of*  
636 *Hydrogen Energy* **2016**, *41* (42), 19484–19491. <https://doi.org/10.1016/j.ijhydene.2016.02.053>.
- 637 (42) Pallozzi, V.; Di Carlo, A.; Bocci, E.; Villarini, M.; Foscolo, P. U.; Carlini, M. Performance Evaluation  
638 at Different Process Parameters of an Innovative Prototype of Biomass Gasification System  
639 Aimed to Hydrogen Production. *Energy Conversion and Management* **2016**, *130*, 34–43.  
640 <https://doi.org/10.1016/j.enconman.2016.10.039>.
- 641 (43) Marcantonio, V.; De Falco, M.; Capocelli, M.; Bocci, E.; Colantoni, A.; Villarini, M. Process  
642 Analysis of Hydrogen Production from Biomass Gasification in Fluidized Bed Reactor with

- 643 Different Separation Systems. *International Journal of Hydrogen Energy* **2019**, *44* (21), 10350–  
644 10360. <https://doi.org/10.1016/j.ijhydene.2019.02.121>.
- 645 (44) Ribeiro, A. M.; Santos, J. C.; Rodrigues, A. E. Pressure Swing Adsorption for CO<sub>2</sub> Capture in  
646 Fischer-Tropsch Fuels Production from Biomass. *Adsorption* **2011**, *17* (3), 443–452.  
647 <https://doi.org/10.1007/s10450-010-9280-8>.
- 648 (45) Pelletier, C.; Rogaume, Y.; Dieckhoff, L.; Bardeau, G.; Pons, M.-N.; Dufour, A. Effect of  
649 Combustion Technology and Biogenic CO<sub>2</sub> Impact Factor on Global Warming Potential of Wood-  
650 to-Heat Chains. *Applied Energy* **2019**, *235*, 1381–1388.  
651 <https://doi.org/10.1016/j.apenergy.2018.11.060>.
- 652 (46) François, J.; Fortin, M.; Patisson, F.; Dufour, A. Assessing the Fate of Nutrients and Carbon in the  
653 Bioenergy Chain through the Modeling of Biomass Growth and Conversion. *Environmental  
654 Science & Technology* **2014**, *48* (23), 14007–14015. <https://doi.org/10.1021/es5032823>.
- 655 (47) Debal, M.; Girods, P.; Rogaume, Y. Wood Gasification in a Semi-Industrial Bubbling Fluidized  
656 Bed Gasifier. In *7th international symposium on gasification and its applications*; Nancy, 2021.
- 657 (48) AspenTech. *Aspen Physical Property Methods*; 2013; p 250.
- 658 (49) Rönsch, S.; Wagner, H. Calculation of Heating Values for the Simulation of Thermo-Chemical  
659 Conversion Plants with Aspen Plus. *DBFZ. Germany* **2012**.
- 660 (50) Corella, J.; Toledo, J. M.; Molina, G. Calculation of the Conditions to Get Less than 2 g Tar/Mn<sub>3</sub>  
661 in a Fluidized Bed Biomass Gasifier. *Fuel Processing Technology* **2006**, *87* (9), 841–846.  
662 <https://doi.org/10.1016/j.fuproc.2006.05.002>.
- 663 (51) Smith, A. R.; Klosek, J. A Review of Air Separation Technologies and Their Integration with  
664 Energy Conversion Processes. *Fuel Processing Technology* **2001**, *70* (2), 115–134.  
665 [https://doi.org/10.1016/S0378-3820\(01\)00131-X](https://doi.org/10.1016/S0378-3820(01)00131-X).
- 666 (52) Ding, Z.; Han, Z.; Qiang, F.; Shen, Y.; Tian, C.; Zhang, D. Optimization and Analysis of the VPSA  
667 Process for Industrial-Scale Oxygen Production. *Adsorption* **2018**, *24*, 499–516.  
668 <https://doi.org/10.1007/s10450-018-9956-z>.
- 669 (53) Santos Silva Ferreira, D. A. High-Purity Oxygen Production by VPSA. Ph.D. Dissertation,  
670 University of Porto, 2016.
- 671 (54) Dufour, A. Optimisation de la production d'hydrogène par conversion du méthane dans les  
672 procédés de pyrolyse/gazéification de la biomasse, Université Henri Poincaré, Nancy, 2007.
- 673 (55) Gil, J.; Corella, J. Biomass Gasification in Atmospheric and Bubbling Fluidized Bed: Effect of the  
674 Type of Gasifying Agent on the Product Distribution. *Biomass and Bioenergy* **1999**, *15*.
- 675 (56) Debiagi, P. E. A.; Gentile, G.; Pelucchi, M.; Frassoldati, A.; Cuoci, A.; Faravelli, T.; Ranzi, E.  
676 Detailed Kinetic Mechanism of Gas-Phase Reactions of Volatiles Released from Biomass  
677 Pyrolysis. *Biomass and Bioenergy* **2016**, *93*, 60–71.  
678 <https://doi.org/10.1016/j.biombioe.2016.06.015>.
- 679 (57) Dhahak, A.; Bounaceur, R.; Le Dreff-Lorimier, C.; Schmidt, G.; Trouve, G.; Battin-Leclerc, F.  
680 Development of a Detailed Kinetic Model for the Combustion of Biomass. *Fuel* **2019**, *242*, 756–  
681 774. <https://doi.org/10.1016/j.fuel.2019.01.093>.
- 682 (58) Norinaga, K.; Deutschmann, O.; Saegusa, N.; Hayashi, J. Analysis of Pyrolysis Products from Light  
683 Hydrocarbons and Kinetic Modeling for Growth of Polycyclic Aromatic Hydrocarbons with  
684 Detailed Chemistry. *Journal of Analytical and Applied Pyrolysis* **2009**, *86* (1), 148–160.  
685 <https://doi.org/10.1016/j.jaap.2009.05.001>.
- 686 (59) Norinaga, K.; Shoji, T.; Kudo, S.; Hayashi, J. Detailed Chemical Kinetic Modelling of Vapour-Phase  
687 Cracking of Multi-Component Molecular Mixtures Derived from the Fast Pyrolysis of Cellulose.  
688 *Fuel* **2013**, *103*, 141–150. <https://doi.org/10.1016/j.fuel.2011.07.045>.
- 689 (60) Kraussler, M.; Binder, M.; Fail, S.; Bosch, K.; Hackel, M.; Hofbauer, H. Performance of a Water  
690 Gas Shift Pilot Plant Processing Product Gas from an Industrial Scale Biomass Steam Gasification  
691 Plant. *Biomass and Bioenergy* **2016**, *89*, 50–57.  
692 <https://doi.org/10.1016/j.biombioe.2015.12.001>.

- 693 (61) Yousef, R.; Qiblawey, H.; El-Naas, M. H. Adsorption as a Process for Produced Water Treatment:  
694 A Review. *Processes* **2020**, *8* (12), 1657. <https://doi.org/10.3390/pr8121657>.
- 695 (62) Yuan, M.; Tong, S.; Zhao, S.; Jia, C. Q. Adsorption of Polycyclic Aromatic Hydrocarbons from  
696 Water Using Petroleum Coke-Derived Porous Carbon. *Journal of Hazardous Materials* **2010**, *181*  
697 (1–3), 1115–1120. <https://doi.org/10.1016/j.jhazmat.2010.05.130>.
- 698 (63) Rabou, L. P. L. M.; Zwart, R. W. R.; Vreugdenhil, B. J.; Bos, L. Tar in Biomass Producer Gas, the  
699 Energy Research Centre of The Netherlands (ECN) Experience: An Enduring Challenge. *Energy*  
700 *Fuels* **2009**, *23* (12), 6189–6198. <https://doi.org/10.1021/ef9007032>.
- 701 (64) ECN. Tar Dew Point - Complete Model. 2012.
- 702 (65) Golmakani, A.; Fatemi, S.; Tamnanloo, J. Investigating PSA, VSA, and TSA Methods in SMR Unit  
703 of Refineries for Hydrogen Production with Fuel Cell Specification. *Separation and Purification*  
704 *Technology* **2017**, *176*, 73–91. <https://doi.org/10.1016/j.seppur.2016.11.030>.
- 705 (66) Bounaceur, R.; Berger, E.; Pfister, M.; Ramirez Santos, A. A.; Favre, E. Rigorous Variable  
706 Permeability Modelling and Process Simulation for the Design of Polymeric Membrane Gas  
707 Separation Units: MEMSIC Simulation Tool. *Journal of Membrane Science* **2017**, *523*, 77–91.  
708 <https://doi.org/10.1016/j.memsci.2016.09.011>.
- 709 (67) Ramírez-Santos, Á. A.; Castel, C.; Favre, E. Utilization of Blast Furnace Flue Gas: Opportunities  
710 and Challenges for Polymeric Membrane Gas Separation Processes. *Journal of Membrane*  
711 *Science* **2017**, *526*, 191–204. <https://doi.org/10.1016/j.memsci.2016.12.033>.
- 712 (68) Peters, M. S.; Timmerhaus, K. D.; West, R. E. *Plant Design and Economics for Chemical Engineers*,  
713 fifth edition.; McGraw-Hill New York, 2004.
- 714 (69) Polin, J. P.; Peterson, C. A.; Whitmer, L. E.; Smith, R. G.; Brown, R. C. Process Intensification of  
715 Biomass Fast Pyrolysis through Autothermal Operation of a Fluidized Bed Reactor. *Applied*  
716 *Energy* **2019**, *249*, 276–285. <https://doi.org/10.1016/j.apenergy.2019.04.154>.
- 717 (70) Polin, J. P.; Carr, H. D.; Whitmer, L. E.; Smith, R. G.; Brown, R. C. Conventional and Autothermal  
718 Pyrolysis of Corn Stover: Overcoming the Processing Challenges of High-Ash Agricultural  
719 Residues. *Journal of Analytical and Applied Pyrolysis* **2019**, *143*, 104679.  
720 <https://doi.org/10.1016/j.jaap.2019.104679>.
- 721 (71) Dufour, A.; Valin, S.; Castelli, P.; Thiery, S.; Boissonnet, G.; Zoulalian, A.; Glaude, P.-A.  
722 Mechanisms and Kinetics of Methane Thermal Conversion in a Syngas. *Ind. Eng. Chem. Res.*  
723 **2009**, *48* (14), 6564–6572. <https://doi.org/10.1021/ie900343b>.
- 724